Electronic Supplementary Material (ESI) for Chemical Communications.

Supporting Information

Twist it! The Acid-Dependent Isomerization of Homoleptic Carbenic Iridium(III) Complexes

Jaroslaw G. Osiak[†a], Tobias Setzer[†b], Peter G. Jones[c], Christian Lennartz[d], Andreas Dreuw[e], Wolfgang Kowalsky[a], Hans-Hermann Johannes*[a]

[a] M. Sc. J. G. Osiak, Prof. Dr.-Ing. W. Kowalsky, Dr. H.-H. Johannes
Institut für Hochfrequenztechnik, Technische Universität Braunschweig
Bienroder Weg 94, 38106 Braunschweig (Germany)
E-Mail: h2.johannes@ihf.tu-bs.de

[b] M. Sc. T. Setzer
BASF SE, GOM/CQ – B009, 67056 Ludwigshafen am Rhein (Germany)

[c] Prof. Dr. P. G. Jones
Institut für Anorganische und Analytische Chemie, Technische Universität Braunschweig, Hagenring 30, 38106 Braunschweig (Germany)

[d] Dr. C. Lennartz
trinamiX GmbH
Industriestraße 35, 67063 Ludwigshafen (Germany)

[e] Prof. Dr. A. Dreuw
Interdisciplinary Center for Scientific Computing, Ruprecht-Karls Universität Heidelberg
Im Neuenheimer Feld 205A, 69120 Heidelberg (Germany)
Email: andreas.dreuw@iwr.uni-heidelberg.de

[†] These authors contributed equally to this publication

Experimental protocols and analytical data

Content

1. General remarks

Solvents and reagents were purchased from Acros, Alfa Aesar, Sigma Aldrich or TCI and were used without further purification unless otherwise stated. Flash column chromatography (FC) purification was performed using “Kieselgel 60M” (Merck) or Aluminium oxide (Sigma Aldrich, activated, neutral, Brockmann activity I). The aluminium oxide was deactivated to Brockmann activity III prior to use.
All reactions were carried out under inert gas conditions.

2. Analytical instruments and annotations

The following methods and instruments were used for the analysis of the synthesized materials

Mass spectrometry: Thermofinnigan MAT95XL (EI) and ThermoFisher Scientific LTQ-Orbitrap Velos (ESI). The ionization was carried out using the negative mode.
Nuclear magnetic resonance spectroscopy (NMR): 600 MHz (^{1}H), 151 MHz (^{13}C): Bruker AV2-600 spectrometer; 400 MHz (^{1}H), 100 MHz (^{13}C): Bruker DRX-400; 200 MHz (^{1}H), 50 MHz (^{13}C): Varian Oxford 200. ^{1}H chemical shifts (δ in ppm) were either referenced to tetramethylsilane (TMS) or to the corresponding solvent signal. ^{13}C measurements were taken with the corresponding solvent signal as the reference. $J_{H,H}$ values are rounded to 0.1 Hz. Abbreviations for the multiplicities are: singlet (s), doublet (d), doublet of doublets (dd), doublet of doublets of doublets (ddd), doublet of triplets (dt), triplet (t), triplet of doublets (td), quartet (q), quintet (quint), sextet (sextet), septet (septet), multiplet (m), and broad (br).

Melting Points: These were either determined by a Stuart Melting Point SMP 3 or by differential scanning calorimetry (DSC) using a Metler Toledo - DSC 1 Star^{e} System. For DSC measurements a sample of the material was placed in a 40 µL aluminum pan, during the analysis the sample is under a constant nitrogen stream of 50 L x min^{-1}. The temperature program for the analysis consists of the following steps: 1. 25 – 150 °C, 10 °C x min^{-1}; 2. 150 °C, 20 min; 3. 150 – 500 °C, 10 °C x min^{-1}; 500 °C, 5 min; 500 – 25 °C, -10 °C x min^{-1}.

High performance liquid chromatography: Knauer Degaser; Knauer WellChrom Solvent Organizer K-1500; Knauer WellChrom HPLC Pump K-1001; Knauer Dynamic Mixing Chamber; Knauer Smartline Autosampler 3950; Techlab column oven; Waters Symmetry C8 5 µm 4.6 x 250 mm; Knauer Smartline PDA Detector 2800.

The column was constantly kept at 22 °C. A gradient elution using the following parameters allowed us to separate the geometrical isomers of the complexes chromatographically:

Time [min]	Water [%]	THF[%]	Flow [mL • min^{-1}]
Initial	50	50	1.000
15	30	70	1.000
20	10	90	1.000
22	5	95	1.000
23	50	50	1.000

Thin layer chromatography: Silica plates (Polygram SIL G/UV 254), Alox

3. Synthetic Protocols

3.1. Synthesis of 1-phenyl-1*H*-benzo[*d*]imidazole

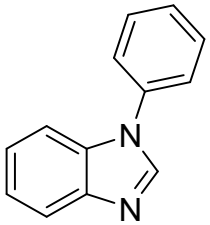

In a 250 mL round bottom flask 10.534 g (51.634 mmol) iodobenzene, 5.000 g (42.323 mmol) benzimidazole, 7.838 g (51.634 mmol) K_2CO_3 and 1.491 g (7.830 mmol) CuI are added to 65 mL of DMF. The reaction is stirred for 72 h under reflux and then cooled to room temperature. After 48 h of reaction time another portion of 1.195 g (10.115 mmol) benzimidazole is added. The reaction mixture is then filtered through a Büchner funnel using celite and the residue washed with portions of DCM. Then the solvent of the filtrate is removed in vacuum and the remaining residue diluted with 100 mL DCM. This solution is washed with aqueous ammonia and then water. The organic phase is dried over $MgSO_4$ and the solvent removed in vacuum. The product is a yellow oil (7.136 g, 36.739 mmol, 87%).
NMR:

^{1}H-NMR (400 MHz, $CDCl_3$) δ [ppm]: 8.12 (s, 1H), 7.92 – 7.86 (m, 1H), 7.60 – 7.42 (m, 6H), 7.37 – 7.29 (m, 2H).

^{13}C-NMR (100 MHz, $CDCl_3$) δ [ppm]: 143.8, 142.2, 136.2, 133.6, 130.0, 128.0, 123.9, 123.6, 122.7, 120.5, 110.4.

ESI-MS (ACN:Toluene 1:1): *m*/*z* calcd. [M+H, $C_{13}H_{10}N_2$+H]$^+$ 195.09222, found 195.09176.

3.2. Synthesis of 3-methyl-1-phenyl-1*H*-benzo[*d*]imidazolium iodide

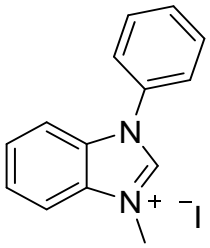

In a 100 ml round bottom flask 2.500 g (12.871 mmol) 1-phenyl-1*H*-benzo[*d*]imidazole is dissolved in 32 mL THF. The reaction solution is stirred at room temperature while 9.134 g (64.353 mmol) methyl iodide is slowly added via a syringe pump at 0.24 ml/min. The reaction is stirred for 24 h at 70 °C and then allowed to cool to room temperature. During the reaction time the product precipitates from the solution and is afterwards filtered of. The remaining residue is washed with portions of THF and then dried in high vacuum overnight. The product is a white amorphous powder (3.883 g, 11.551 mmol, 90%).

^{1}H-NMR (600 MHz, DMSO-D_6) δ [ppm]: 10.15 (d, $J_{H,H}$ = 0.4 Hz, 1H), 8.17 (td, $J_{H,H}$ = 8.4, 0.9 Hz, 1H), 7.87 – 7.82 (m, 3H), 7.82 – 7.70 (m, 5H), 4.18 (s, 3H).

^{13}C-NMR (150 MHz, DMSO-D_6) δ [ppm]: 143.0 (d), 133.1 (s), 131.8 (s), 130.8 (s), 130.4 (d), 127.4 (d), 126.8 (d), 125.0 (d), 113.9 (d), 113.3 (d), 33.5 (q).

Melting point: 200.8 °C

ESI-MS (MeOH): *m*/*z* calcd. [M–I, $C_{14}H_{13}N_2^+$]$^+$ 209.10732, found 209.10734.

This compound was previously described and characterized by Forrest et al.[1]

3.3. Synthesis of 3-benzyl-1-phenyl-1*H*-benzo[*d*]imidazolium bromide

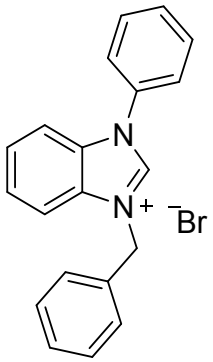

A 50 mL pressure tube is charged with 0.800 g (4.119 mmol) 1-phenyl-1*H*-benzo[*d*]imidazole, 5 mL THF and a stirring bar. After addition of 0.845 g (4.942 mmol) benzylbromide the pressure tube is sealed carefully and the reaction mixture heated to 100 – 110°C. The reaction mixture is stirred for 24 h and then allowed to cool to room temperature. The precipitate is filtered off with suction and washed with portions of THF. The product is dried in high vacuum overnight. The product is a white amorphous powder (1.159 g, 3.172 mmol, 77%).

NMR: ^{1}H-NMR (600 MHz, DMSO-D_6) δ [ppm]: 10.47 (s, 1H), 8.05 – 8.03 (m, 1H), 7.91 (dd, $^{3}J_{H,H}$ = 8.4 Hz, $^{4}J_{H,H}$ = 1.1 Hz, 1H), 7.90 (dd, $^{3}J_{H,H}$ = 8.4 Hz, $^{4}J_{H,H}$ = 1.1 Hz, 1H), 7.87 (dd, $^{3}J_{H,H}$ = 7.3 Hz, $^{4}J_{H,H}$ = 2.8 Hz, 1H), 7.80 – 7.76 (m, 2H), 7.75 – 7.73 (m, 1H), 7.73 – 7.72 (m, 1H), 7.72 – 7.71 (m, 1H), 7.66 (d, $^{3}J_{H,H}$ = 6.9 Hz, 2H), 7.44 (tt, $^{3}J_{H,H}$ = 8.3 Hz, $^{4}J_{H,H}$ = 1.8 Hz, 2H), 7.40 (t, $^{3}J_{H,H}$ = 7.3 Hz, 1H), 5.89 (s, 2H).

^{13}C-NMR (150 MHz, DMSO-D_6) δ [ppm]: 142.8 (d, C-1), 133.6 (s, C-15), 133.1 (s, C-8), 131.3 (s, C-7), 130.8 (s, C-2), 130.4 (d, C-11), 130.3 (d, C-10/12), 128.9 (d, C-17/19), 128.7 (d, C-18), 128.4 (d, C-16/20), 127.4 (d, C-5), 127.0 (d, C-6), 125.2 (d, C-9/13), 114.2 (d, C-3), 113.7 (d, C-4), 50.2 (t, C-14).

Melting point: 206.3 °C.

ESI-MS (MeOH): *m*/*z* calcd. [M–Br, $C_{20}H_{17}N_2^+$]$^+$ 285.13862, found 285.13880.

This compound was previously described and characterized by Strassner et al.[2]

3.4. Synthesis of tris(*N*-phenyl,*N*-methyl-benzimidazol-2-yl)iridium(III) (1)

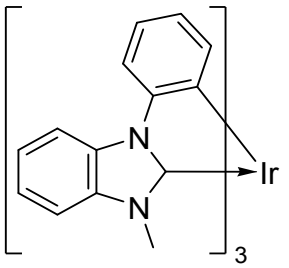

In a 250 ml round bottom flask 3.498 g (10.406 mmol) 3-benzyl-1-methyl-1*H*-benzo[*d*]imidazolium iodide is dissolved in 160 ml 1,4-dioxane. Afterwards 0.571 g (2.464 mmol) silver(I)oxide is added and the residues rinsed down by addition of 10 mL 1,4-dioxane. The reaction is stirred overnight at 60 °C. Thereafter 0.699 g (1.041 mmol) bis(1,5-cyclooctadiene)diiridium(I) dichloride is added, the reaction temperature elevated to 120 °C and the mixture stirred for another 24 h. The reaction is then allowed to cool to room temperature and the precipitate filtered off. Removal of the filtrate solvent gives a crude product, which is further purified by FC (Al_2O_3 (III), DCM:*n*-Hexane 1:2, R_f = 0.3). A white powder with a slight yellowish tinge is obtained (0.942 g, 1.157 mmol, 56%)

^{1}H-NMR (600 MHz, DMSO-D_6) δ [ppm]: 8.37 (d, $J_{H,H}$ = 7.9 Hz, 1H), 8.36 (d, $^4J_{H,H}$ = 7.9 Hz, 1H), 8.29 (d, $J_{H,H}$ = 8.3 Hz, 1H), 7.97 (d, $J_{H,H}$ = 7.9 Hz, 1H), 7.95 (d, $J_{H,H}$ = 7.9 Hz), 7.88 (dd, $J_{H,H}$ = 8, 0.7 Hz, 1H), 7.54 (d, $J_{H,H}$ = 7.8 Hz, 1H), 7.50 (d, $J_{H,H}$ = 8.1 Hz, 1H), 7.48 (dd, $J_{H,H}$ = 8.1, 0.7 Hz, 1H), 7.29 – 7.40 (m, 6H), 6.96 – 6.90 (m, 3H), 6.74 (d, $J_{H,H}$ = 7 Hz, 2H), 6.60 – 6.58 (m, 3H), 6.44 (dd, $J_{H,H}$ = 7.2, 1.5 Hz, 1H), 3.28 (s, 3H), 3.21 (s, 3H), 3.17 (s, 3H).

^{13}C-NMR (150 MHz, DMSO-D_6) δ [ppm]: 187.8 (s), 184.5 (s), 184.1 (s), 151.3 (s), 149.5 (s), 149.4 (s), 148.4 (s), 147.5 (s), 147.2 (s), 138.4 (d), 138.0 (d), 136.2 (d), 136.1 (s), 136.1 (s), 135.8 (s), 131.5 (s), 124.7 (d), 124.3 (d), 123.9 (d), 123.2 (d), 123.2 (d), 123.1 (d), 122.2 (d), 122.2 (d), 122.1 (d), 121.0 (d), 120.4 (d), 120.3 (d), 112.4 (d), 112.3 (d), 112.1 (d), 111.3 (d), 111.2 (d), 111.0 (d), 110.7 (d), 110.7 (d), 110.7 (d), 33.2 (q), 33.2 (q), 32.4 (q).

Melting point: No melting point was detected. Decomposition starts at 375.5 °C.
ESI-MS (ACN:Toluene 1:1): *m*/*z* calcd. [M, $C_{42}H_{33}IrN_6$]$^+$ 814.23959, found 814.23956.
This compound was previously described and characterized by Forrest et al.[1]

3.5. Synthesis of tris(*N*-phenyl,*N*-benzyl-benzimidazol-2-yl)iridium(III) (2)

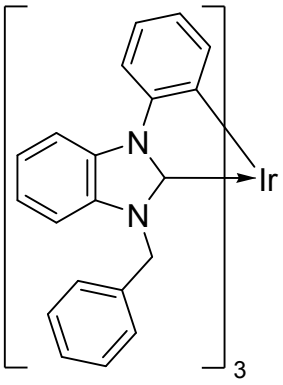

In a 250 ml round bottom flask 1.800 g (4.928 mmol) 3-benzyl-1-phenyl-1*H*-benzo[*d*]imidazolium bromide is dissolved in 75 ml 1,4-dioxane. Afterwards 0.571 g, (2.464 mmol) silver(I)oxide is added and the residues rinsed down by addition of 7 mL 1,4-dioxane. The reaction is stirred overnight at 60 °C. Thereafter 0.331 g (0.493 mmol) bis(1,5-cyclooctadiene)diiridium(I) dichloride is added, the reaction temperature elevated to 120 °C and the mixture stirred for another 24 h. The reaction is then allowed to cool to room temperature and the precipitate filtered off. Removal of the filtrate solvent gives a crude product, which is further purified by FC (Al_2O_3 (III), DCM:*n*-Hexane 1:2, R_f = 0.3). A white powder with a slight yellowish tinge is obtained (0.734g, 0.704 mmol, 72%)

^{1}H-NMR (600 MHz, THF-D_8) δ [ppm]: 8.13 (d, $J_{H,H}$ = 8.3 Hz, 1H), 7.77 (d, $J_{H,H}$ = 8.5 Hz, 1H), 7.76 (d, $J_{H,H}$ = 7.9 Hz, 1H), 7.36 (dd, $J_{H,H}$ = 7.5, 1.0 Hz, 1H), 7.32 (dd, $J_{H,H}$ = 8.0, 0.7 Hz, 1H), 7.15 (ddd, $J_{H,H}$ = 8.4, 5.8, 2.7 Hz, 1H), 7.10 – 7.06 (m, 2H), 7.02 – 6.95 (m, 4H), 6.90 – 6.87 (m, 1H), 6.85 (td, $J_{H,H}$ = 7.5, 1.2 Hz, 1H), 6.83 – 6.78 (m, 3H), 6.75 – 6.60 (m, 6H), 6.60 – 6.54 (m, 3H), 6.48 – 6.39 (m, 7H), 6.24 (dd, $J_{H,H}$ = 8.2, 0.9 Hz, 2H), 6.15 (d, $J_{H,H}$ = 8.5 Hz, 2H), 6.13 (d, $J_{H,H}$ = 8.1 Hz, 2H), 5.44 (d, $J_{H,H}$ = 16.3 Hz, 1H), 5.38 (d, $J_{H,H}$ = 16.2 Hz, 1H), 5.31 (d, $J_{H,H}$ = 16.8 Hz, 1H), 5.00 (d, $J_{H,H}$ = 16.8 Hz, 1H), 4.85 (d, $J_{H,H}$ = 16.2 Hz, 1H), 4.67 (d, $J_{H,H}$ = 16.3 Hz, 1H).

^{13}C-NMR (150 MHz, THF-D_8) δ [ppm]: 191.0 (s), 186.7 (s), 186.4 (s), 152.0 (s), 150.9 (s), 149.9 (s), 149.8 (s), 149.0 (s), 147.6 (s), 139.5 (d), 139.0 (d), 137.8 (d), 137.6 (s), 137.2 (s), 137.0 (s), 136.3 (s), 133.9 (s), 133.8 (s), 133.6 (s), 128.5 (d), 128.3 (d), 128.2 (d), 127.3 (d), 127.1 (d), 127.0 (d), 126.5 (d), 126.2 (d), 125.8 (d), 125.4 (d), 125.1 (d), 124.8 (d), 123.6 (d), 123.3 (d), 122.8 (d), 122.6 (d), 122.5 (d), 122.2 (d), 121.2 (d),

121.0 (d), 120.7 (d), 113.8 (d), 113.6 (d), 113.2 (d), 112.6 (d), 112.6 (d), 112.2 (d), 111.5 (d), 111.3 (d), 111.0 (d), 51.3 (t), 51.2 (t), 51.2 (t).

Melting point: 337.8 °C

ESI-MS (ACN:Toluene 1:1): *m*/*z* calcd. [M, $C_{60}H_{45}IrN_6]^+$ 1042.33349, found 1042.33506.

3.6. Isomerization of tris(*N*-phenyl,*N*-methyl-benzimidazol-2-yl)iridium(III) (1)

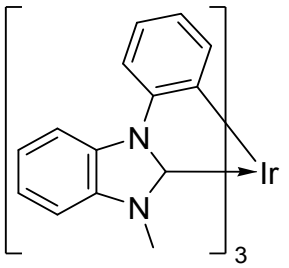

The EtOAc used for this reaction is degassed with nitrogen prior to use.
Inside an argon glovebox a 100 mL pressure tube is filled with 0.425 g (0.522 mmol) *mer*-tris(*N*-phenyl,*N*-methyl-benzimidazol-2-yl)iridium(III), which is then dissolved in 53 mL EtOAc. After addition of 5.2 mL (1M in H_2O) malonic acid the pressure tube is sealed carefully and removed from the box. The reaction is heated to 65°C for 6 d. The progress of the reaction is indicated by precipitation of the *fac* complex. Afterwards the reaction mixture is allowed to cool to room temperature, the precipitate is filtered off with suction and washed with portions of EtOAc. A white solid is obtained and dried in high vacuum (0.231 g, 0.284 mmol, 54%).

^{1}H-NMR (600 MHz, THF-D_8) δ [ppm]: 8.11 (d, $J_{H,H}$ = 8.2 Hz, 3H), 7.74 (dd, $J_{H,H}$ = 8.0, 0.8 Hz, 3H), 7.18 (d, $J_{H,H}$ = 8.0 Hz, 3H), 7.15 (ddd, $J_{H,H}$ = 8.4, 7.5, 1.2 Hz, 3H), 7.07 (ddd, $J_{H,H}$ = 8.2, 7.5, 0.9 Hz, 3H), 6.78 (ddd, $J_{H,H}$ = 7.9, 7.3, 1.6, 3H), 6.50 (dd, $J_{H,H}$ = 7.3, 1.5 Hz, 3H), 6.40 (dt, $J_{H,H}$ = 7.3, 1.0 Hz, 3H), 3.18 (s, 9H).

^{13}C-NMR (150 MHz, THF-D_8) δ [ppm]: 191.1 (s), 150.0 (s), 149.4 (s), 137.9 (d), 137.4 (s), 133.6 (s), 124.9 (d), 123.3 (d), 122.3 (d), 121.4 (d), 112.6 (d), 111.8 (d), 110.6 (d), 33.6 (q).

Melting point: 462.5 °C.

ESI-MS (MeOH): *m*/*z* calcd. [M, $C_{42}H_{33}IrN_6$]$^+$ 814.23959, found 814.23962.

This compound was previously described and characterized by Forrest et al.[1]

3.7. Isomerization of tris(*N*-phenyl,*N*-benzyl-benzimidazol-2-yl)iridium(III) (2)

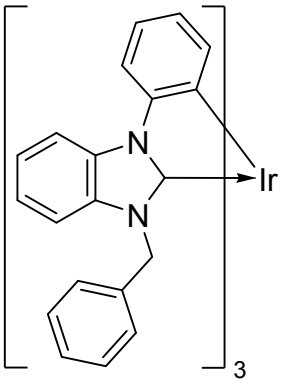

The EtOAc used for this reaction is degassed with nitrogen prior to use.
Inside an argon glovebox a 100 mL pressure tube is filled with 0.500 g (0.480 mmol) *mer*-tris(*N*-phenyl,*N*-methyl-benzimidazol-2-yl)iridium(III), which is then dissolved in 53 mL EtOAc. After addition of 4.9 mL (1M in H_2O) trifluoroacetic acid the pressure tube is sealed carefully and removed from the box. The reaction is heated to 65°C for 15 h. The progress of the reaction is indicated by precipitation of the *fac* complex. Afterwards the reaction mixture is allowed to cool to room temperature, the precipitate is filtered off with suction and washed with portions of EtOAc. A white solid is obtained and dried in high vacuum (0.380 g, 0.365 mmol, 76%).

^{1}H-NMR (600 MHz, THF-D_8) δ [ppm]: 7.72 (d, $J_{H,H}$ = 8.3 Hz, 3H), 7.53 (dd, $J_{H,H}$ = 8.0, 0.8 Hz, 3H), 6.96 (ddd, $J_{H,H}$ = 8.4, 7.4, 1.2 Hz, 3H), 6.86 (ddd, $J_{H,H}$ = 8.1, 7.4, 0.8 Hz, 3H), 6.83 – 6.77 (m, 9H), 6.65 – 6.62 (m, 6H), 6.52 (dd, $J_{H,H}$ = 7.3, 1.5 Hz, 3H), 6.43(td, $J_{H,H}$ = 7.3, 1.0 Hz, 3H), 6.08 (d, $J_{H,H}$ = 7.4 Hz, 6H), 5.23 (d, $J_{H,H}$ = 16.6 Hz, 3H), 4.80 (d, $J_{H,H}$ = 16.5 Hz, 3H).

^{13}C-NMR (150 MHz, DMSO-D_6) δ [ppm]: 191.4 (s), 150.1 (s), 149.3 (s), 137.5 (d), 136.6 (s), 136.2 (s), 133.8 (s), 128.7 (d), 127.4 (d), 126.0 (d), 124.9 (d), 123.1 (d), 122.2 (d), 121.4 (d), 113.3 (d), 112.2 (d), 110.8 (d), 52.0 (t).

Melting point: 378.8 °C.

ESI-MS (ACN:Toluene 1:1): *m*/*z* calcd. [M, $C_{60}H_{45}IrN_6]^+$ 1042.33349, found 1042.33382.

5. Theoretical Contribution

Assuming a first-order reaction[3] for the studied intramolecular transformations, likely and unlikely mechanistic pathways can be distinguished by calculating the activation barrier for a given half-life $t_{\frac{1}{2}}$ of a unimolecular reaction and a given temperature. For our intramolecular isomerizations we consider a reaction scenario relevant if $t_{\frac{1}{2}} < 12\ h$ .This means that $\Delta G^{\ddagger} < 113\ kJ/mol$ for $T = 60\ °C$ and $\Delta G^{\ddagger} = 109\ kJ/mol$ for $T = 50\ °C$. Although not all reaction steps are of first order, most of the reactions are of first order with respect to the iridium complex so that typically pseudo-first order kinetics apply in the presence of reactants that have a much higher concentration.

$\Delta G^{\circ,\ddagger}\left(t_{\frac{1}{2}},T\right) = ln(k_{t_{\frac{1}{2}}}h/k_B T)\cdot(-RT)$ with $k_{t_{\frac{1}{2}}} = \ln(2)/t_{\frac{1}{2}}$

5.1. Computational Details

Molecular structures were optimized at the BP86-D3/def2-SV(P) level of theory using the resolution of identity approximation (RI) together with suitable auxiliary basis functions.[4–10] Absolute electronic energies E_{el} were obtained by performing B3LYP-D3/def2-TZVP single-point calculations.[4,6–11]

In general electronic structure calculations were carried out with the TURBOMOLE program package, employing effective core potentials (ECPs) for iridium.[12,13]

Statistical corrections to the gas-phase energies (within the well established rigid-rotor and harmonic oscillator approximations), ΔG_{stat}, were calculated at the BP86-D3/def2-SV(P) level for the reaction conditions $T = 60\ °C$ and $p = 1\ bar$ using the *freeh* program included in TURBOMOLE package. For the constitutional isomers of *fac*-**2** (see 5.2) only, the calculated reaction conditions were $T = 50\ °C$ and $p = 1\ bar$. Symmetry numbers in the rotational partition functions according to the molecular symmetry were taken into account. All (positive) vibrational frequencies were included in the calculation of the vibrational partition function in order to qualitatively account for entropic contributions stemming from a sterically crowded ligand sphere. However, the presence of low vibrational frequencies and the restricted validity of the harmonic oscillator approximation (high reaction temperatures) limit the accuracy of the present study.

Free enthalpies of solvation, $^{\Delta G_{solv,SP}}$, in ethyl acetate solution were obtained within the COSMO-RS model and the parametrization for BP86/def-TZVP using the COSMOtherm program.[11,12] To this end the calculation of the BP86/def-TZVP/COSMO as well as the corresponding gas-phase energy is required. Computation of the solvation free energies using the gas-phase optimized structures is in general sufficient. The reference state in this work is defined for $T = 60\,°C$ and $\chi = 1.0$ for which an ideally diluted solution is assumed (*fac*-**2** constitutional isomers $T = 50\,°C$ and $\chi = 1.0$, see 5.2). For the ethyl acetate solvent four different conformers were included in the COSMO-RS model (see 5.5)

Following a procedure outlined in the literature[16] the total Gibbs free energies presented here for each species are obtained as $G_{total} = E_{el} + \Delta G_{stat} + \Delta G_{solv,SP}$. In general all free energies are given in kJ/mol and relative to the common reference point G_{total}(**I**$) + G_{total}(CF_3COOH) = G_{ref} = 0.0\ kJ/mol$ defined in the context. Free energies that do not refer to this reference point are denoted ΔG and are separately defined in the text.

The transition state search presented in this work was carried out manually by scanning relevant reaction trajectories that connect the considered intermediates. Along the cut through the energy surface one of the structures at (or close to) the energetical maximum was chosen as a guess structure for a transition state optimization. Therefore the Hessian of this structure was calculated and a structure optimization along an imaginary mode corresponding to the trajectory of interest was performed. In order to evaluate that the obtained transition state connects starting materials and products, once again a Hessian was calculated and the remaining imaginary mode was inspected visually.

5.2. Deuteration experiment and Quantum chemical calculations

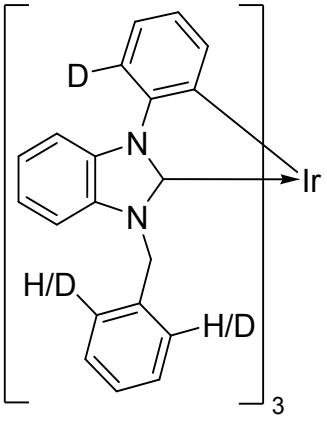

In a 10 mL vial 0.030 g (0.029 mmol) *mer*-**2** was dissolved in 3.7 mL EtOAc and after addition of 0.37 mL deuterated trifluoroacetic acid (1M in D_2O) stirred for 32 d at 50 °C. The reaction was monitored by HPLC. The precipitate is filtered off, dried and analysed by NMR.

SI-Fig. 1 shows the ^{1}H-NMR spectra of *fac*-**2** compared to the complex that is obtained by using the deuterated acid. While the signal at 7.5 ppm, which is assigned to the phenyl proton at position 6, completely vanishes, the peak at 6.1 ppm, associated with the benzylic protons at positions 2 and 6, only decreases by roughly 50 %. Accordingly, there is evidence that a reversible bond-rupture (deuteration followed by cyclometallation) occurs at phenyl-carbon 6. On the other hand the deuteration at the benzylic positions 2 and 6 does not clearly indicates a cyclometallation followed by a subsequent deuteration of the benzyl moiety to the iridium center. Owing to the very long reaction time it is more likely that the corresponding base (CF_3COO^-) partially abstracts the benzylic protons at the benzylic positions 2 and 6, respectively.

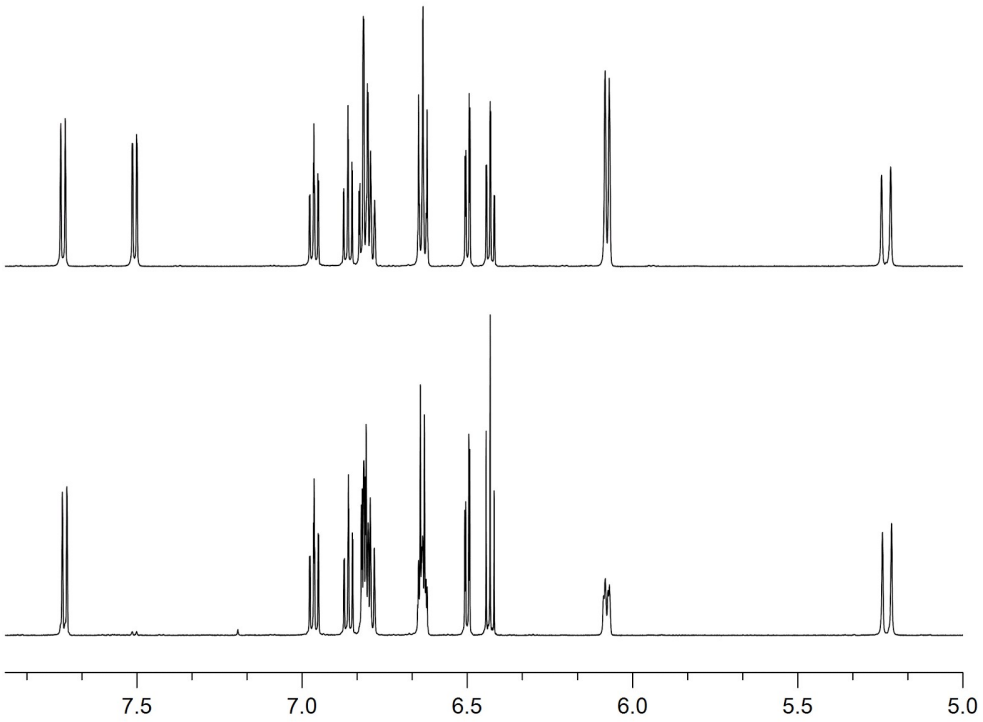

SI-Fig. 1: ^{1}H-NMR of an undeuterated *fac*-2 sample (top) and a deuterated *fac*-2 sample (bottom).

The results of our quantum chemical calculations shown in SI-Fig. 2 clearly confirm the findings of the deuteration experiment, in that *fac*-**2** ($G = -3.8\ kJ/mol$)is the lowest energy species, closely followed by the reference point *mer*-**2** ($G = 0.0\ kJ/mol$). The energetically most favourable constitutional isomer having at least one benzyl moiety linked to the iridium center is **D4** with $G = 44.7\ kJ/mol$. Due to the observed reversible protonation and cyclometallation reaction for the phenylic hydrogen at position 6 it is not only reasonable to start the mechanistic investigation by assuming a bond-rupture isomerization mechanism as proposed by Amati and Lelj[17], but it also proves how straightforwardly the whole isomerization reaction proceeds in direction of *fac*-**2**. Although some byproducts or intermediates showing benzyl-iridum linkages might possibly occur in very minor portions their influence on the productive minimal energy pathway can be neglected since no reduction of energy barriers can be expected from their inclusion in the mechanistic considerations. This systematic exclusion of substituent based effects on the reaction mechanism confirms the use of methyl-substituted **I** (*mer*-**1**) as a prototypical test system to be meaningful: There is no evidence that the ligand system's substitution pattern (methyl *vs.* benzyl) could potentially lead to different isomerization mechanisms of the two complexes **1** and **2**.

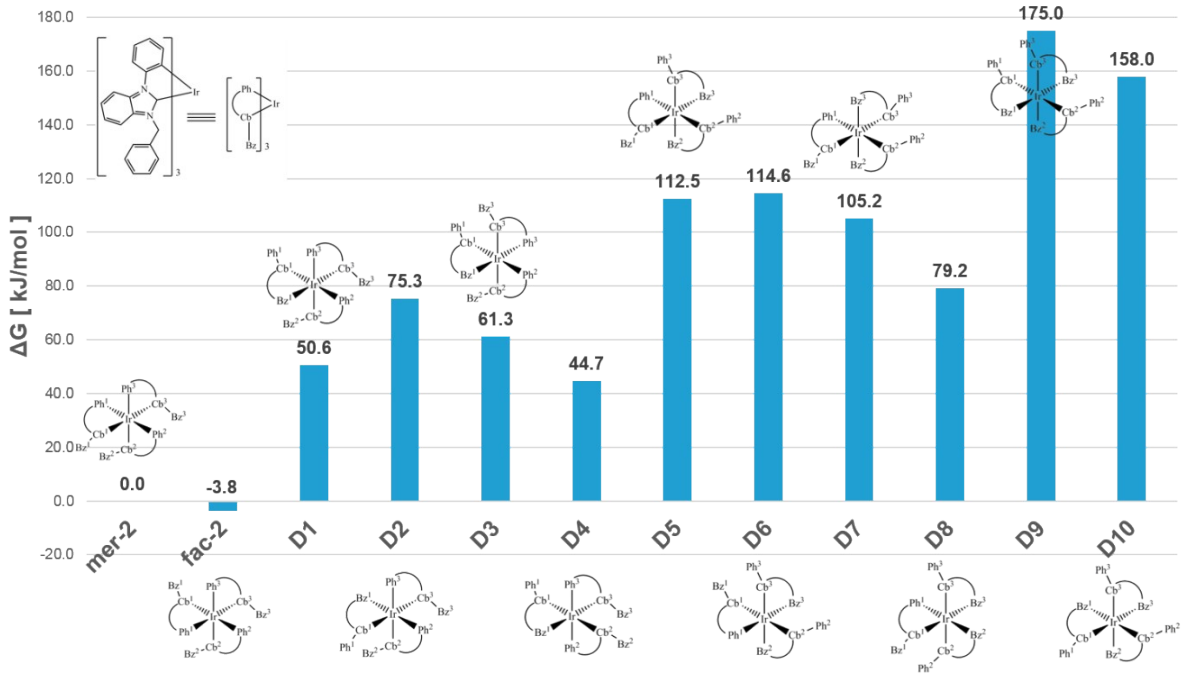

SI-Fig. 2: Calculation of all possible configuration isomers of *fac*-**2**.

5.3. Conformational analysis of malonic acid/acetate

While for HCl/Cl^- and CF_3COOH/CF_3COO^- no conformational analysis is needed, the most relevant planar and nonplanar conformations of malonic acid ($C_3H_4O_4$) and malonic (mono-)acetate ($C_3H_3O_4^-$) were tested. Monomeric malonic acid has been studied previously by *ab initio* (Hartree-Fock (HF), Møller-Plesset (MP)) and Density Functional Theory (DFT) vacuum calculations. HF/6-31G(d), MP2/6-31G(d,p) and MP2/6-311++G(2d,2p) predict the non-planar form II (SI-Fig. 3) to be the most stable conformation, whereas B3LYP with the 6-31G(d,p), 6-311++G(2d,2p) and 6-311++G(3df,3pd) basis predicts the planar form I (SI-Fig. 3) with intramolecular hydrogen bonds to be the most stable conformer. Since the MP2/6-311++G(3df,3pd) results (including a large and diffuse basis set) confirm the B3LYP findings and predict the planar form I to be energetically favoured over form II the authors finally conclude form I to be slightly more stable than form II.[18] Based on the electronic energies we obtained by B3LYP-D3/def2-TZVP and BP86-D3/def2-SV(P) calculations these findings (planar form I is more stable than the twisted form II by 8.8 kJ/mol in electronic energy) can be confirmed. On the other hand when environmental effects are taken into account according to our Gibbs free energy calculation procedure a stabilization of the twisted form II over the planar form I by $^{\Delta G_{acid}(twisted-planar)} = -8.0\ kJ/mol$ is observed. Because these results are only qualitatively comparable with previous vacuum calculations[18] and the influence of hydrogen-bond interactions with EtOAc that are accounted for in the COSMO-RS model are hard to quantify, we show the results for both the planar and the twisted form of malonic acid in SI-Fig. 3.

To obtain an insight as to which conformational form the coordinated malonate will adopt in the Ir(III) intermediate **II,** we also tested the same planar and nonplanar conformation as for the acid. Not only electronic energies at the B3LYP-D3/def2-TZVP and BP86-D3/def2-SV(P) level, but also Gibbs free energy calculations predict the planar conformation with an intramolecular hydrogen bond to be by far the most stable conformer ($^{G_{acetate}(twisted-planar)} = 39.4\ kJ/mol$). This observation is in perfect agreement with an earlier work on conformers of monoanionic malonic acetate.[19] Therefore we prepared **II** linking a planar malonate with internal hydrogen bond (malonate form I**,** SI-Fig. 3) to the vacant Ir(III) coordination site and optimized the structure according to the above-mentioned procedure (see Ch. 5.1).

Summarizing, the influence of the two different conformers of malonic acid is only accounted for on the educt side of the reaction equation **I** + HX → **II** (see SI-Fig. 6 or

scheme 2 of the article), where the vacant coordination site of **II** is always occupied by a planar malonate of form I (see. SI-Fig. 3). For HX on the other hand form I and form II of malonic acid were tested as is discussed in the article.

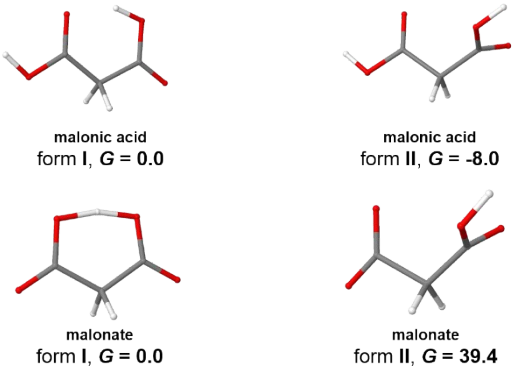

SI-Fig. 3: Conformers of malonic acid and malonate used within this study.

5.4. Solvation effects of HCl in ethyl acetate

Besides the conformational issues shown above for malonic acid/malonate, we also addressed the microsolvation effect of hydrochloric acid in ethyl acetate using the COSMO-RS model.[20] As shown in the upper reaction scheme of SI-Fig. 4 we compared the net reaction of **I** to **II** using pure HCl (compare SI-Fig. 6) with the same reaction (lower scheme in SI-Fig 4) including one explicit *trans*-ethyl acetate solvent molecule (**k1**) interacting with HCl *via* hydrogen bonding. The interaction of HCl with the ethyl acetate solvent is only considered for the starting materials, since there is no explicit interaction between the product chloro-complex and an ethyl acetate molecule (for instance no acidic protons to interact with the coordinated chloride). Therefore ethyl acetate (**k1**) only acts as a spectator on the product side of the lower reaction scheme of SI-Fig. 4. By comparing the upper and the lower reaction scheme in SI-Fig. 4 we find that the differences in Gibbs free energies between the products and the starting materials only differ by 3 kJ/mol.

Therefore it is perfectly reasonable to treat HCl as a pure acid and neglect (micro)solvation effects, that means, explicit interactions of the acid with the solvent.

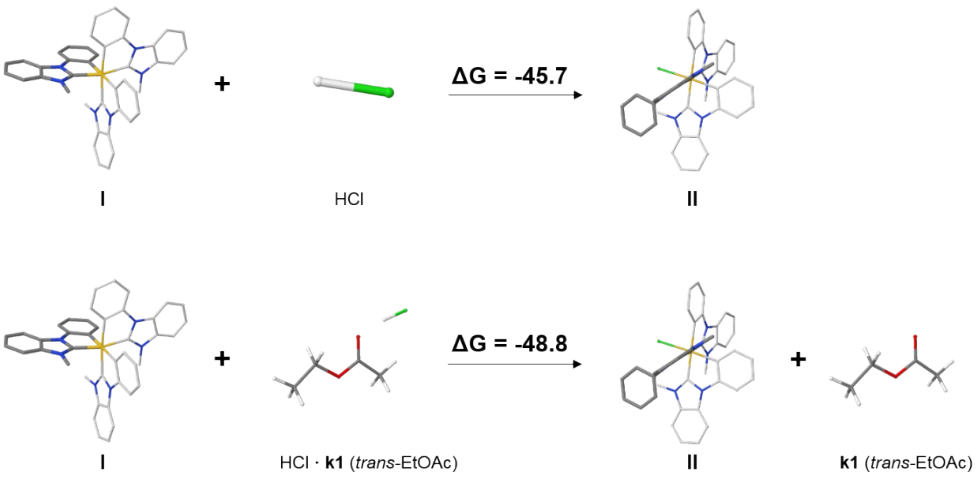

SI-Fig. 4: Testing microsolvation effects of HCl in ethyl acetate.

5.5. Ethyl acetate conformer treatment

Using the COSMO-RS model it is possible to include solvent molecule conformers of interest. Conforming to a recent publication[21] we decided to consider the three lowest-energy conformers **k1** (*trans)*, **k2** (*gauche-1)* and **k3** (*cis).* Additionally, we also included the **k4** (*gauche-2*) conformer. The relative Gibbs free energies of the four conformers (SI-Fig. 5) are calculated according to the Gibbs free energy procedure outlined above (Ch. 5.1) and with respect to the lowest-energy conformer **k1**.

While **k1** (*trans*) and **k2** (*gauche-1*) are close in energy and only differ by 3.4 kJ/mol, **k3** (*cis*) is already significantly higher in energy by 23.7 kJ/mol. In this work we also included the *gauche-2* conformer **k4** in our conformational analysis, and this is the highest energy species *G* = 29.7 kJ/mol.

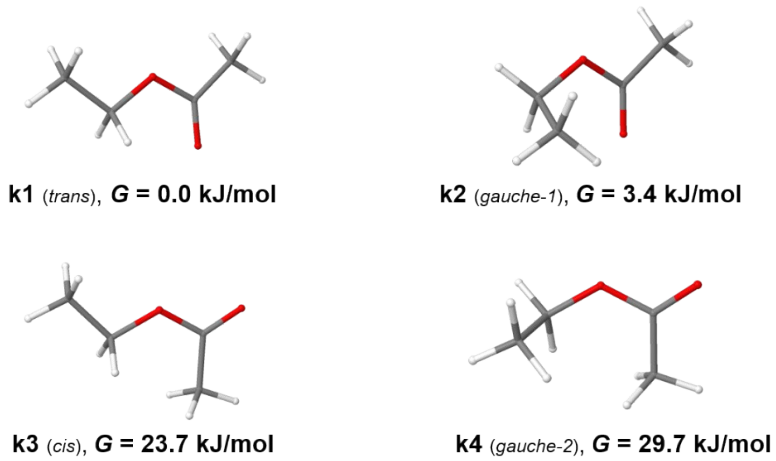

SI-Fig. 5: Conformers of ethyl acetate that are included in the COSMO-RS treatment. Gibbs free energies of all conformers are with respect to **k1**.

5.6. Mechanistic Details

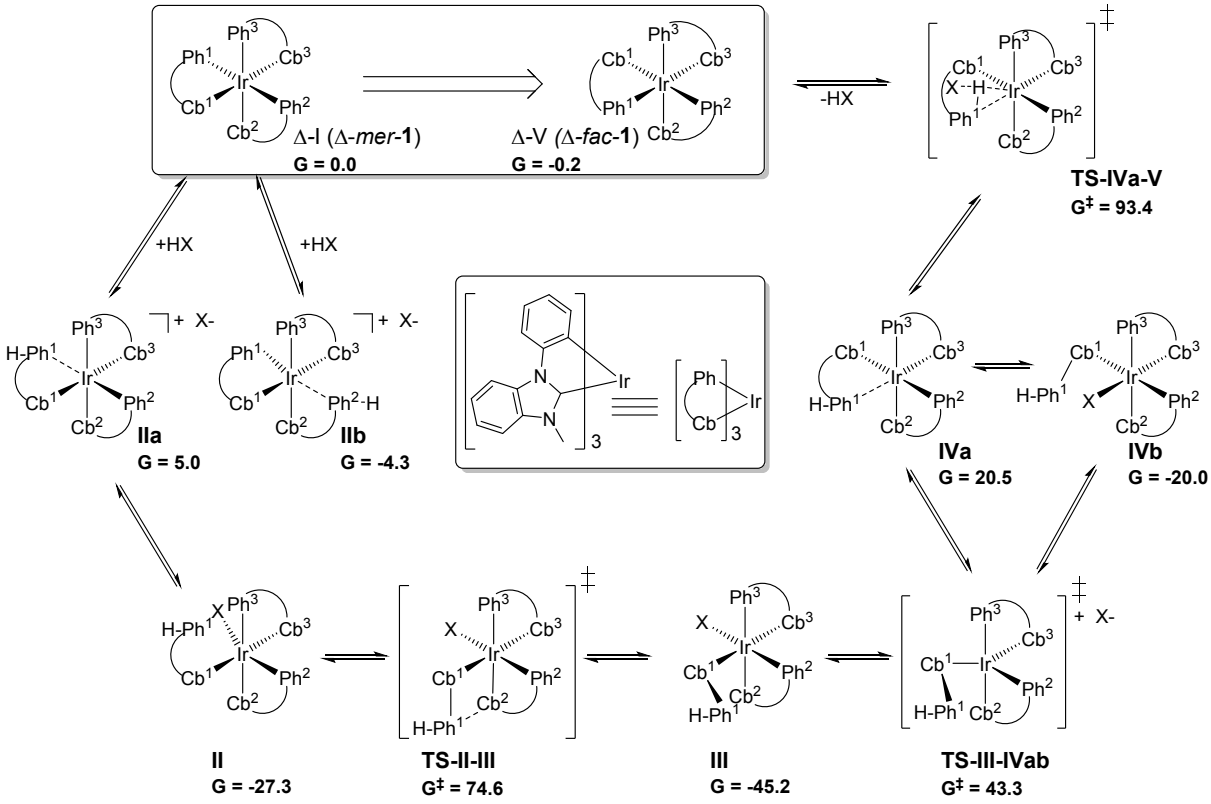

SI-Fig. 6: Complete mechanism including details such as protonated starting species.

5.7. Computational data for thermochemical analysis

Compound	E_{el} [E_h]			ΔG_{stat} [kJ/mol]	$\Delta G_{solv,SP}$ [kJ/mol]	ΔG_{total} [kJ/mol]
	BP86/def2-SV(P) disp3	BP86/def-TZVP	B3LYP/def2-TZVP disp3	BP86/def2-SV(P) vacuum disp3	BP86/def-TZVP COSMO-RS	E_{el}(B3LYP) + ΔG_{stat} + $\Delta G_{solv,SP}$
CF3COO-	-525.89735	-526.52111	-526.29554	-30.43	-203.81	-1382023.17
CF3COOH	-526.43421	-527.04493	-526.82408	3.75	-9.93	-1383182.80
C3H3O4- planar	-416.84928	-417.33594	-417.11797	67.08	-194.97	-1095271.14
C3H4O4 planar	-417.37048	-417.85100	-417.64009	105.26	-29.75	-1096438.56
C3H3O4- twisted	-416.81738	-417.30711	-417.09179	64.36	-221.60	-1095231.72
C3H4O4 twisted	-417.36714	-417.84867	-417.63912	96.48	-31.50	-1096446.53
HCl	-460.69883	-460.86583	-460.76573	-37.15	2.76	-1209774.81
HCl * EtOAc	-768.20399	-768.71233	-768.44448	215.95	-14.60	-2017349.65
EtOAc trans (k1)	-307.48678	-307.83502	-307.66580	201.84	-3.30	-807578.01
EtOAc gauche-1 (k2)	-307.48734	-307.83459	-307.66565	204.15	-2.58	-807574.60
EtOAc cis (k3)	-307.47648	-307.82378	-307.65500	204.71	-10.88	-807554.38
EtOAc gauche-2 (k4)	-307.47583	-307.82241	-307.65377	207.35	-10.68	-807548.30
mer-2	-2745.00628	-2747.51382	-2745.88098	2036.34	-161.09	-7207435.27
fac-2	-2745.00693	-2747.51695	-2745.88231	2038.03	-163.06	-7207439.03
D1	-2744.98965	-2747.49440	-2745.86275	2041.27	-163.29	-7207384.69
D2	-2744.97271	-2747.50236	-2745.85190	2035.19	-161.00	-7207359.98
D3	-2744.97749	-2747.50471	-2745.85496	2032.48	-164.21	-7207373.94
D4	-2744.98904	-2747.50530	-2745.86449	2039.15	-162.54	-7207390.61
D5	-2744.96947	-2747.47537	-2745.84084	2045.54	-163.24	-7207322.82
D6	-2744.96549	-2747.48340	-2745.84052	2043.85	-160.19	-7207320.63
D7	-2744.97265	-2747.48228	-2745.84588	2046.92	-158.63	-7207330.08
D8	-2744.98273	-2747.49067	-2745.85462	2039.53	-154.28	-7207356.06
D9	-2744.95600	-2747.45081	-2745.82223	2050.69	-154.67	-7207260.24
D10	-2744.95965	-2747.45450	-2745.82639	2049.46	-159.52	-7207277.26

I	-2052.26088	-2054.15489	-2052.87273	1434.95	-129.17	-5388511.57
V	-2052.26137	-2054.15427	-2052.87307	1433.00	-126.47	-5388511.72
IIa	-2052.67813	-2054.57164	-2053.29379	1468.39	-211.76	-5389666.22
II	-2578.75241	-2581.21294	-2579.74110	1520.41	-131.84	-6771721.68
II.C3H3O4	-2469.68985	-2472.01612	-2470.55594	1618.25	-139.39	-6484965.76
II.Cl	-2513.01424	-2515.04269	-2513.67978	1472.47	-138.26	-6598332.05
IIb	-2052.68259	-2054.56999	-2053.29574	1467.57	-215.13	-5389675.52

TS-II-III	-2578.71764	-2581.17657	-2579.70392	1526.70	-133.85	-6771619.79
III	-2578.76068	-2581.21812	-2579.74843	1516.98	-127.09	-6771739.61
TS-III-IVab	-2052.66912	-2054.54977	-2053.27977	1472.20	-214.09	-5389627.92
IVa	-2052.67604	-2054.56027	-2053.28812	1472.13	-214.84	-5389650.66
TS-IVa-V	-2578.70050	-2581.16282	-2579.68019	1505.19	-155.77	-6771600.93
IVb	-2578.74162	-2581.20670	-2579.73199	1511.13	-139.12	-6771714.33

6. Crystal Structure Determinations

Crystals were mounted in inert oil on glass fibres and transferred to the cold gas stream of an Oxford Diffraction Xcalibur E diffractometer. Intensities were recorded at 100 K using monochromated Mo $K\alpha$ radiation. Absorption corrections were based on multi-scans. Structures were refined anisotropically on F^2 using the program SHELXL-97[22]. Hydrogen atoms were included using rigid methyl groups or a riding model. Crystal data are summarized in Tables SI 1-3.

Special features and exceptions: Compound fac-**1** crystallizes as a THF disolvate. Compound mer-**2** crystallizes as a THF monosolvate, but the THF is disordered over two positions. A small satellite crystal falsified some intensities, mostly for reflections with l = 3, 5 or 7; these were omitted from the refinement. Repeated attempts to obtain single crystals of compound fac-**2** led only to thin and feathery crystals that were unusable for structure determination. Finally, one attempt using vapour diffusion of di-isopropyl ether into a solution of the compound in THF gave one clump of intergrown blocks. These shattered badly when cut, but one reasonably acceptable fragment was found. The reflection shape was not good, with appreciable smearing and overlap of neighbouring reflections. This is the probable cause of the high residual electron density near the iridium atoms. There is also one peak of ca. 2 e $Å^{-3}$ in a structural void. Compound fac-**2** crystallizes as a THF (2/3)-solvate; the asymmetric unit contains three molecules of fac-**2** and two THF. Because of the large number of parameters, the refinement was based on alternating user-defined blocks; block 1 consisted of the first two independent molecules, block 2 consisted of the third molecule plus the solvent molecules.

Complete data have been deposited at the Cambridge Crystallographic Data Centre under the numbers CCDC-1516674(fac-**1**), -1516675 (mer-**2**), -1516676 (fac-**2**). These data can be obtained free of charge from www.ccdc.cam.ac.uk/data_request/cif.

6.1. Crystal structure of *fac*-(1)

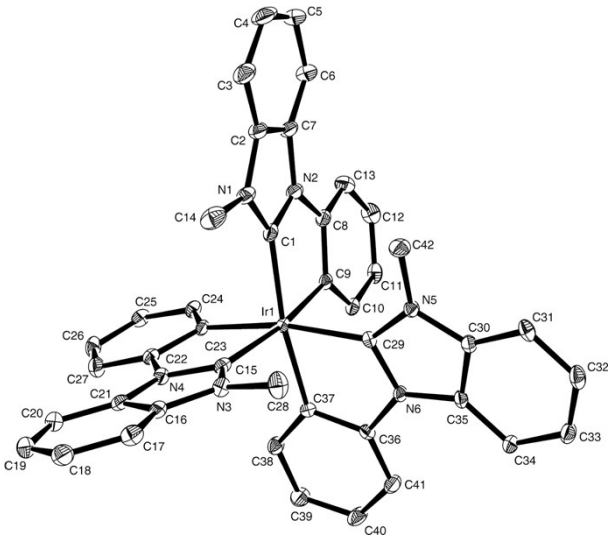

SI-Fig. 7: Single crystal structure of *fac*-(1). Thermal ellipsoids are drawn at 50% probability level. Co-crystallized solvent molecules and hydrogen atoms are omitted.

SI-Table 1: Crystal data and structure refinement for *fac*-(1).

Empirical formula	$C_{50}H_{49}IrN_6O_2$	
Formula weight	958.15	
Temperature	100(2) K	
Wavelength	0.71073 Å	
Crystal system	Monoclinic	
Space group	$P2_1/c$	
Unit cell dimensions	a = 13.0020(3) Å	α= 90°
	b = 18.8143(3) Å	β= 110.919(2)°
	c = 17.6588(4) Å	γ = 90°
Volume	4035.02(15) $Å^3$	
Z	4	
Density (calculated)	1.577 Mg/m^3	
Absorption coefficient	3.359 mm^{-1}	
F(000)	1936	
Crystal size	0.40 x 0.15 x 0.10 mm^3	
Theta range for data collection	2.44 to 31.12°	
Index ranges	-18<=h<=18, -27<=k<=27, -25<=l<=24	
Reflections collected	212736	
Independent reflections	12464 [R(int) = 0.0530]	
Completeness to theta = 30.00°	99.7 %	
Absorption correction	Semi-empirical from equivalents	
Max. and min. transmission	1.00000 and 0.71537	
Refinement method	Full-matrix least-squares on F^2	
Data / restraints / parameters	12464 / 0 / 535	
Goodness-of-fit on F^2	1.149	
Final R indices [I>2sigma(I)]	R1 = 0.0270, wR2 = 0.0563	

R indices (all data)	R1 = 0.0341, wR2 = 0.0585
Largest diff. peak and hole	2.351 and -1.121 e.Å^{-3}

6.2. Crystal structure of *mer*-(2)

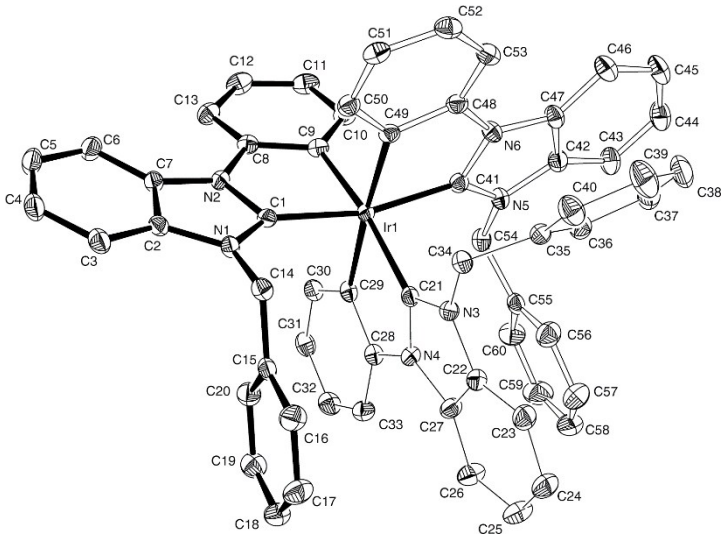

SI-Fig. 8: Single crystal structure of *mer*-(2). Thermal ellipsoids are drawn at 50% probability level. Co-crystallized solvent molecules are omitted.

SI-Table 2. Crystal data and structure refinement for *mer*-(2).

Empirical formula	$C_{64}H_{53}IrN_3O$	
Formula weight	1114.32	
Temperature	100(2) K	
Wavelength	0.71073 Å	
Crystal system	Monoclinic	
Space group	$P2_1/c$	
Unit cell dimensions	a = 20.9475(4) Å	α= 90°
	b = 12.09289(17) Å	β= 106.360(2)°
	c = 20.1184(4) Å	γ = 90°
Volume	4889.96(15) Å^3	
Z	4	
Density (calculated)	1.514 Mg/m^3	
Absorption coefficient	2.783 mm^{-1}	
F(000)	2256	
Crystal size	0.25 x 0.20 x 0.10 mm^3	
Theta range for data collection	2.36 to 31.11°	
Index ranges	-30<=h<=30, -17<=k<=17, -28<=l<=29	
Reflections collected	385454	
Independent reflections	15100 [R(int) = 0.0516]	
Completeness to theta = 30.00°	99.8 %	
Absorption correction	Semi-empirical from equivalents	
Max. and min. transmission	1.00000 and 0.76717	
Refinement method	Full-matrix least-squares on F^2	
Data / restraints / parameters	15100 / 30 / 645	

Goodness-of-fit on F^2	1.081
Final R indices [I>2sigma(I)]	R1 = 0.0263, wR2 = 0.0557
R indices (all data)	R1 = 0.0334, wR2 = 0.0582
Largest diff. peak and hole	1.443 and -0.785 e.$Å^{-3}$

6.3. Crystal structure of *fac*-(2)

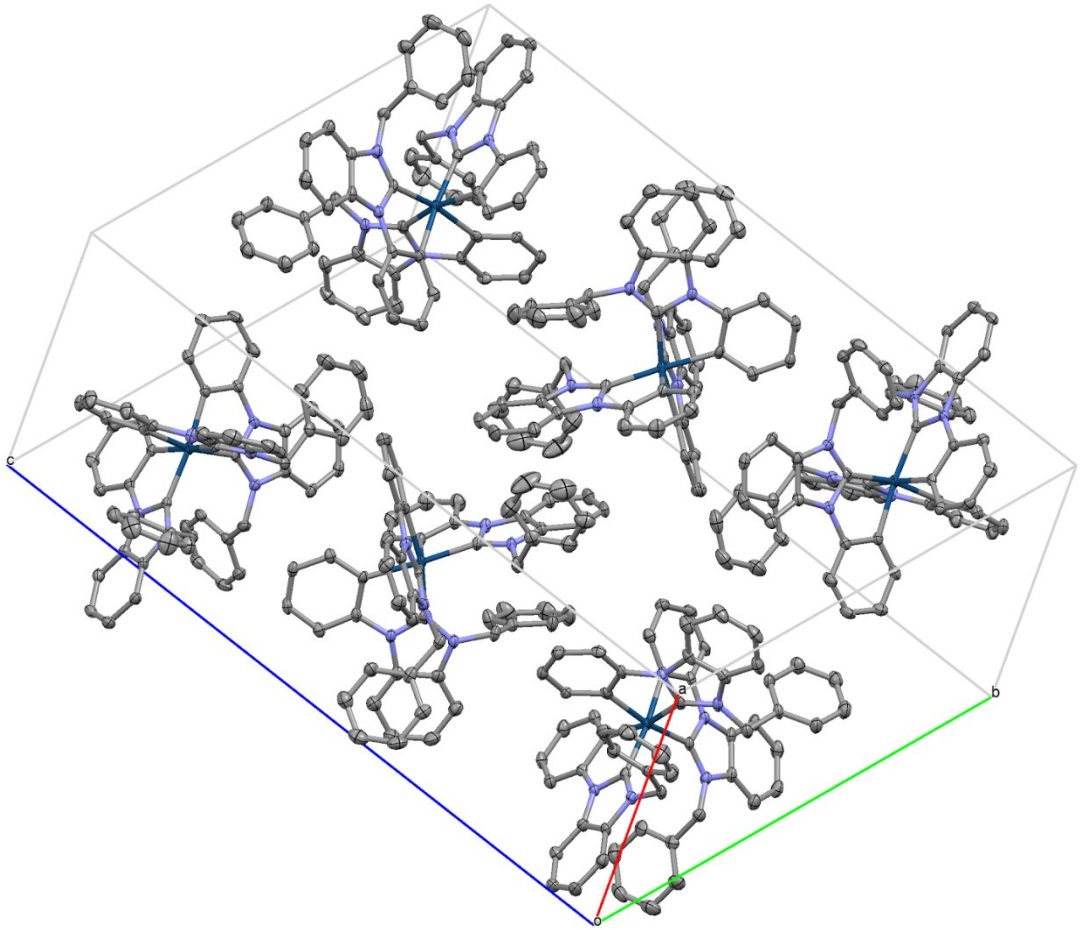

SI-Fig. 9: Single crystal packing diagram for *fac*-(2). Thermal ellipsoids are drawn at 50% probability level. Co-crystallized solvent molecules are omitted.

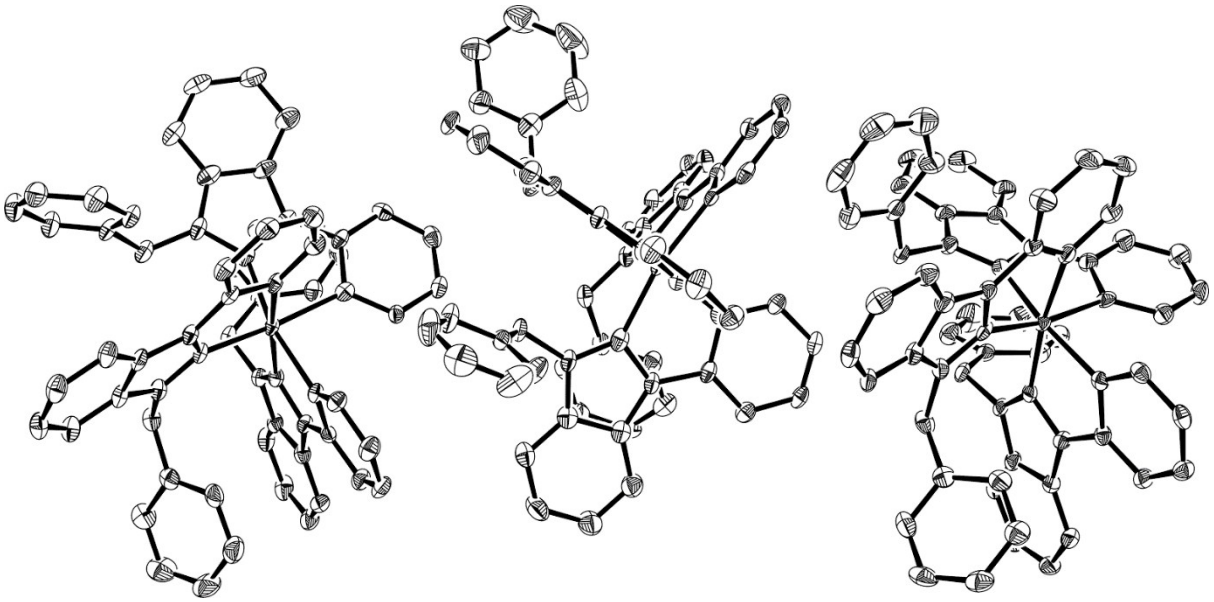

SI-Fig. 10: Single crystal structure of the three independent molecules of *fac*-(2). From left to right: Λ *fac*'-(2), Δ *fac*-(2), Λ *fac*''-(2). Thermal ellipsoids are drawn at 50% probability level. Co-crystallized solvent molecules are omitted.

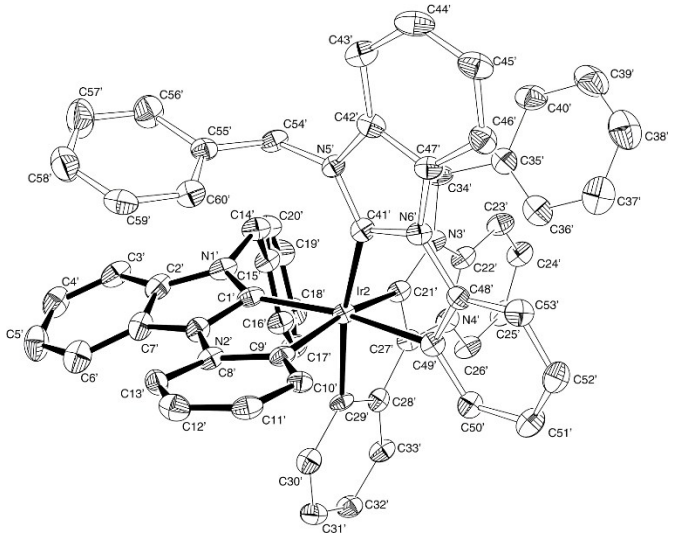

SI-Fig. 11: Single crystal structure of Λ *fac'*-(**2**). Thermal ellipsoids are drawn at 50% probability level. Co-crystallized solvent molecules are omitted.

SI-Table 3. Crystal data and structure refinement for *fac*-(**2**).

Empirical formula	$C_{62.67}H_{50.33}IrN_6O_{0.67}$	
Formula weight	1090.29	
Temperature	100(2) K	
Wavelength	0.71073 Å	
Crystal system	Triclinic	
Space group	P(-1)	
Unit cell dimensions	a = 13.7534(4) Å	α= 95.925(2)°
	b = 19.6098(6) Å	β= 93.542(2)°
	c = 27.0140(5) Å	γ = 94.992(3)°
Volume	7200.9(3) $Å^3$	
Z	6	
Density (calculated)	1.509 Mg/m^3	
Absorption coefficient	2.832 mm^{-1}	
F(000)	3304	
Crystal size	0.4 x 0.3 x 0.2 mm^3	
Theta range for data collection	2.20 to 26.37°	
Index ranges	-17<=h<=17, -24<=k<=24, -33<=l<=33	
Reflections collected	295455	
Independent reflections	29433 [R(int) = 0.0991]	
Completeness to theta = 26.37°	99.9 %	
Absorption correction	Semi-empirical from equivalents	
Max. and min. transmission	1.00000 and 0.86713	
Refinement method	userblock least-squares on F^2	
Data / restraints / parameters	29433 / 0 / 1900	
Goodness-of-fit on F2	1.049	
Final R indices [I>2sigma(I)]	R1 = 0.0430, wR2 = 0.0930	
R indices (all data)	R1 = 0.0626, wR2 = 0.1035	
Largest diff. peak and hole	3.893 and -1.390 $e.Å^{-3}$	

7. NMR Diagrams

7.1. ^{1}H-NMR of 1-phenyl-1*H*-benzo[*d*]imidazole

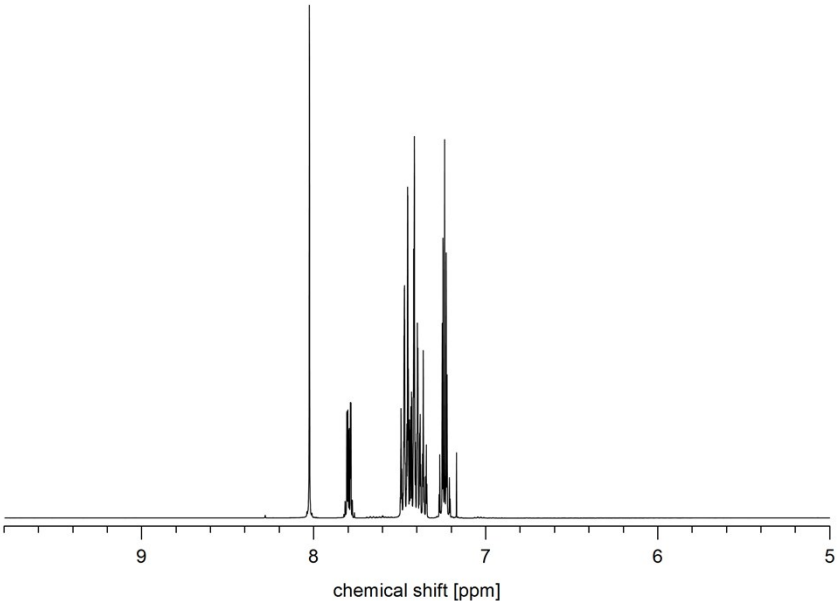

7.2. ^{13}C-NMR of 1-phenyl-1H-benzo[*d*]imidazole

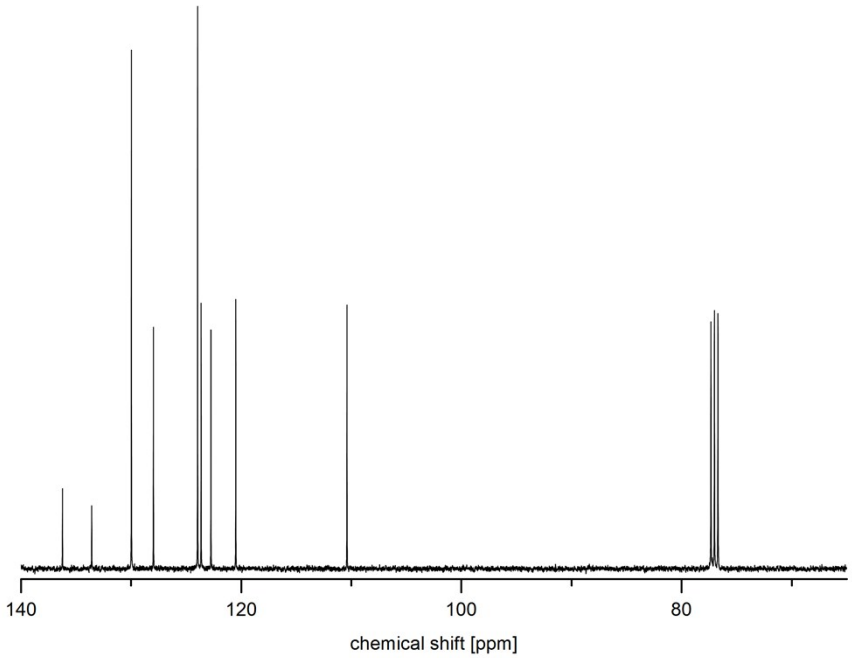

7.3. ^{1}H-NMR of 3-methyl-1-phenyl-1*H*-benzo[*d*]imidazolium iodide

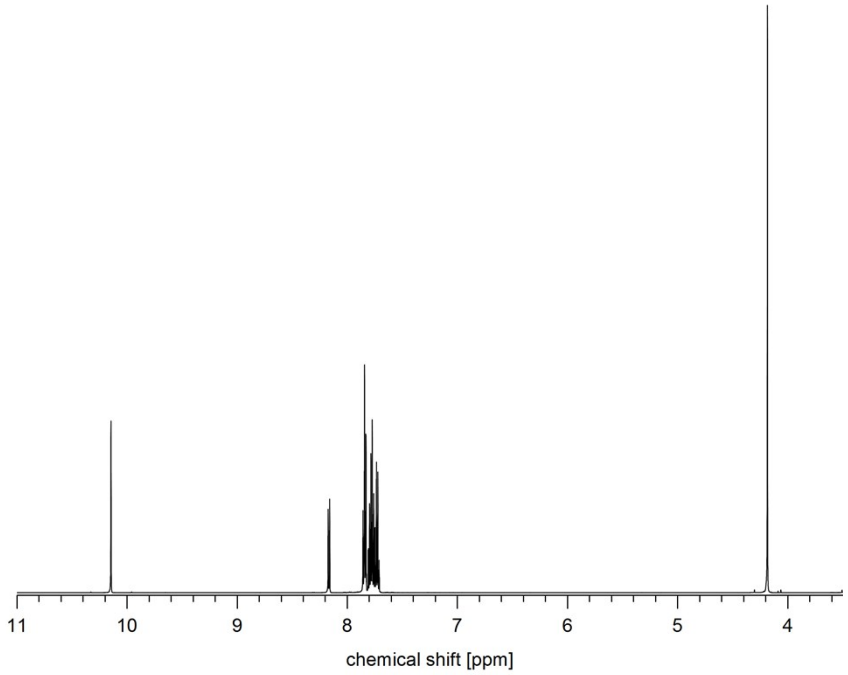

7.4. ^{13}C-NMR of 3-methyl-1-phenyl-1*H*-benzo[*d*]imidazolium iodide

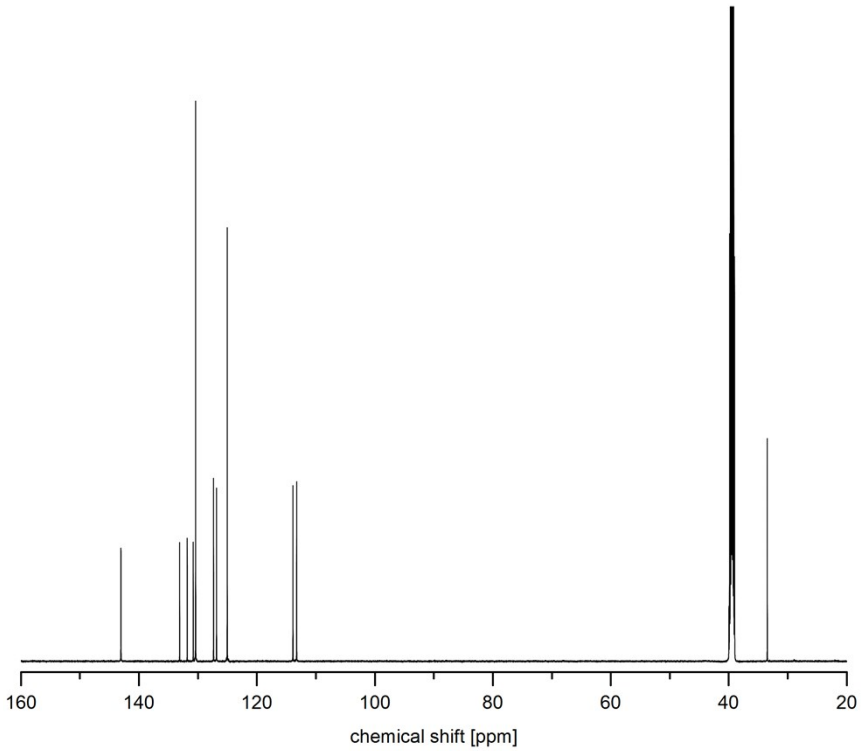

7.5. ^{1}H-NMR of 3-benzyl-1-phenyl-1*H*-benzo[*d*]imidazolium bromide

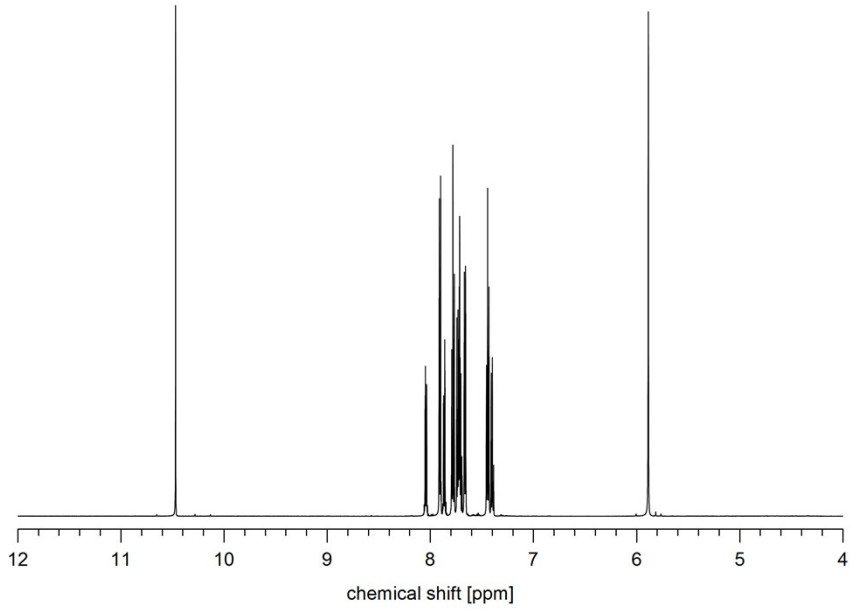

7.6. ^{13}C-NMR of 3-benzyl-1-phenyl-1*H*-benzo[*d*]imidazolium bromide

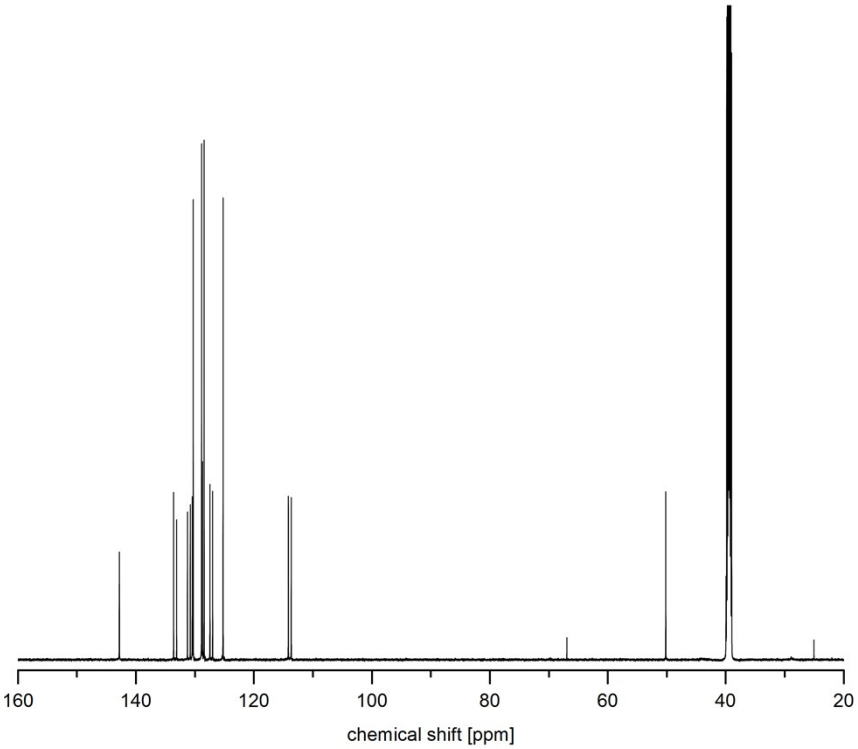

7.7. ^{1}H-NMR of *mer*-tris(*N*-phenyl,*N*-methyl-benzimidazol-2-yl)iridium(III) (1)

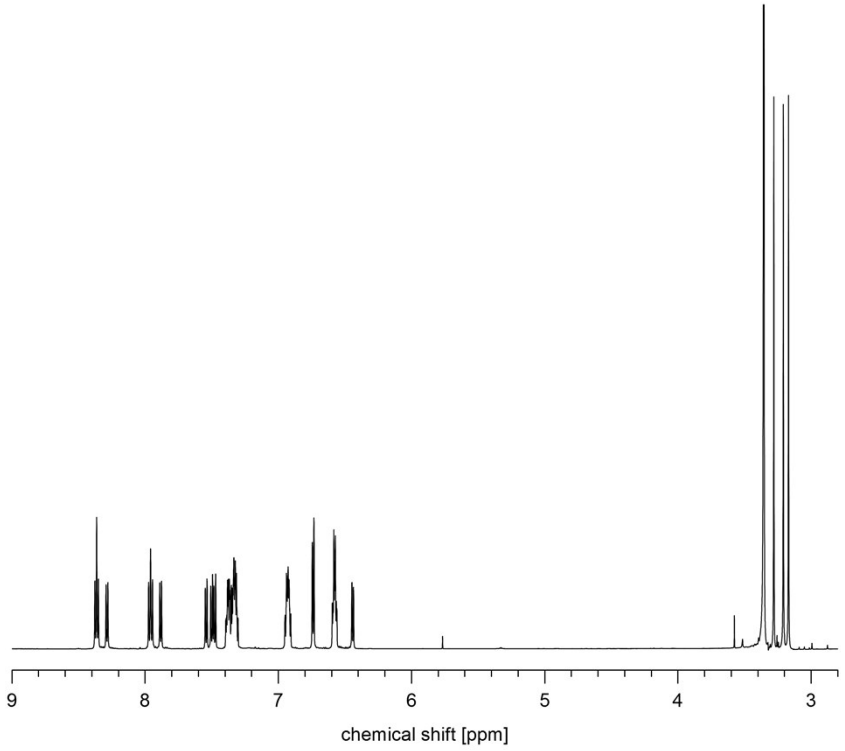

7.8. ^{13}C-NMR of *mer*-tris(*N*-phenyl,*N*-methyl-benzimidazol-2-yl)iridium(III) (1)

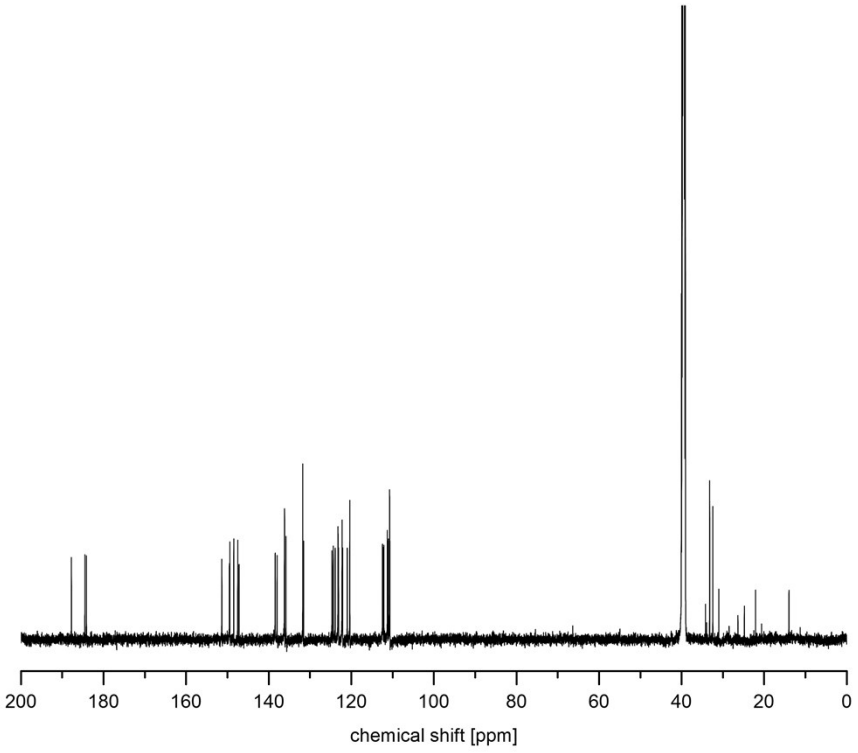

7.9. ^{1}H-NMR of *fac*-tris(*N*-phenyl,*N*-methyl-benzimidazol-2-yl)iridium(III) (1)

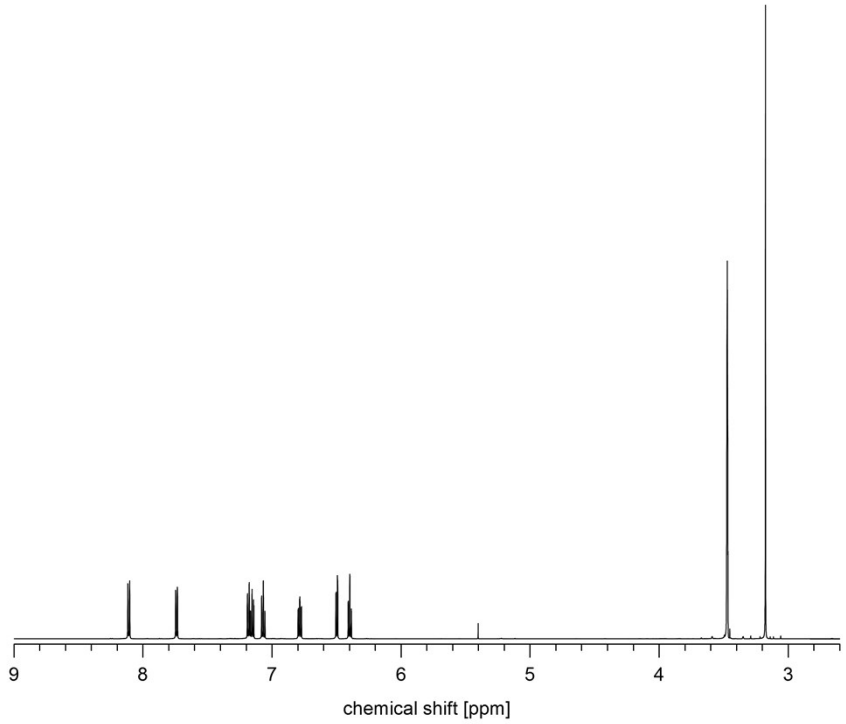

7.10. ^{13}C-NMR of *fac*-tris(*N*-phenyl,*N*-methyl-benzimidazol-2-yl)iridium(III) (1)

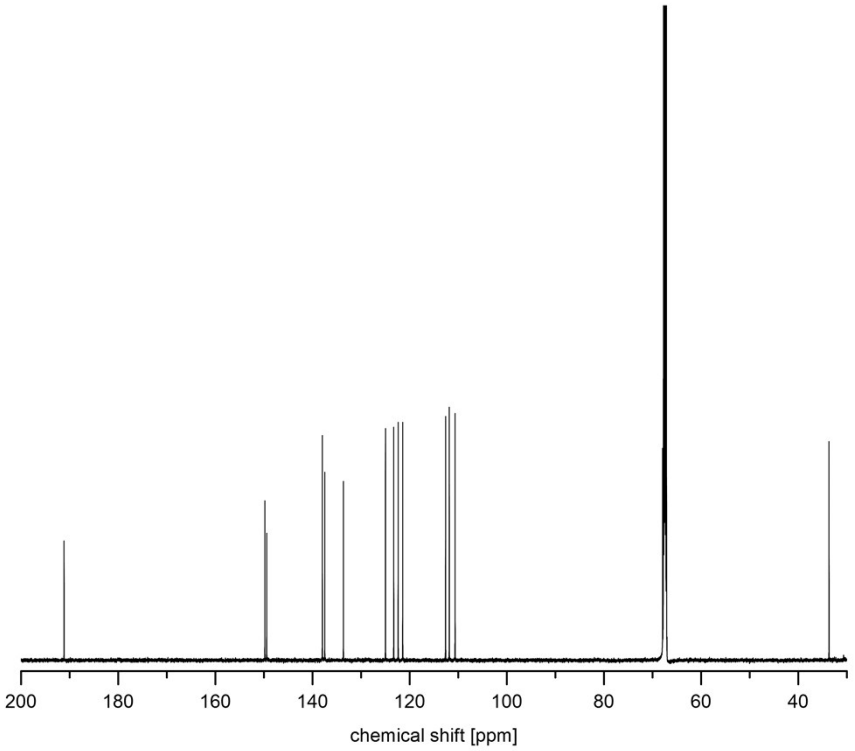

7.11. ^{1}H-NMR of *mer*-tris(*N*-phenyl,*N*-benzyl-benzimidazol-2-yl)iridium(III) (2)

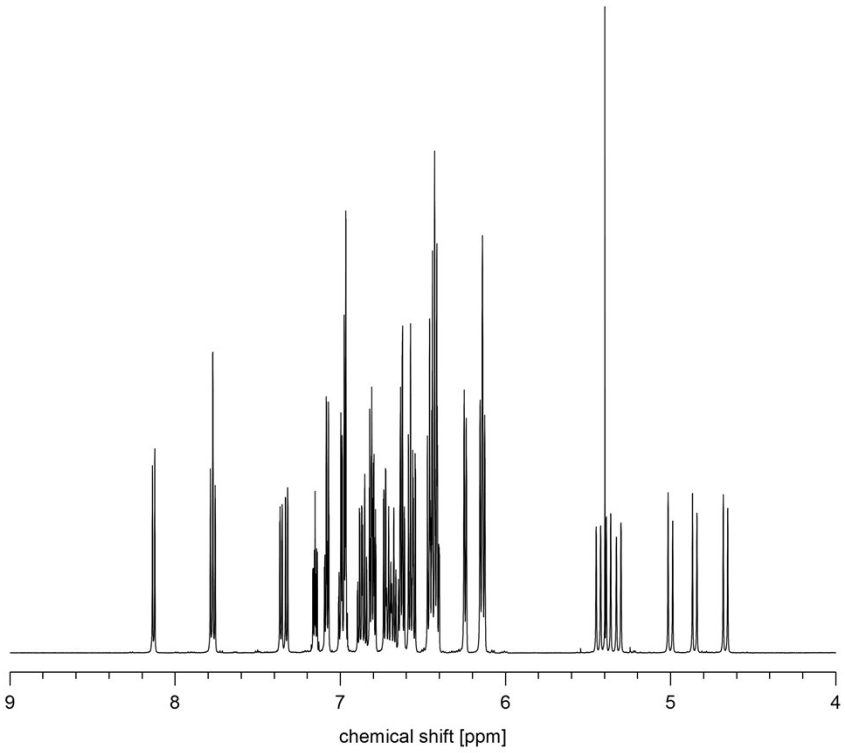

7.12. ^{13}C-NMR of *mer*-tris(*N*-phenyl,*N*-benzyl-benzimidazol-2-yl)iridium(III) (2)

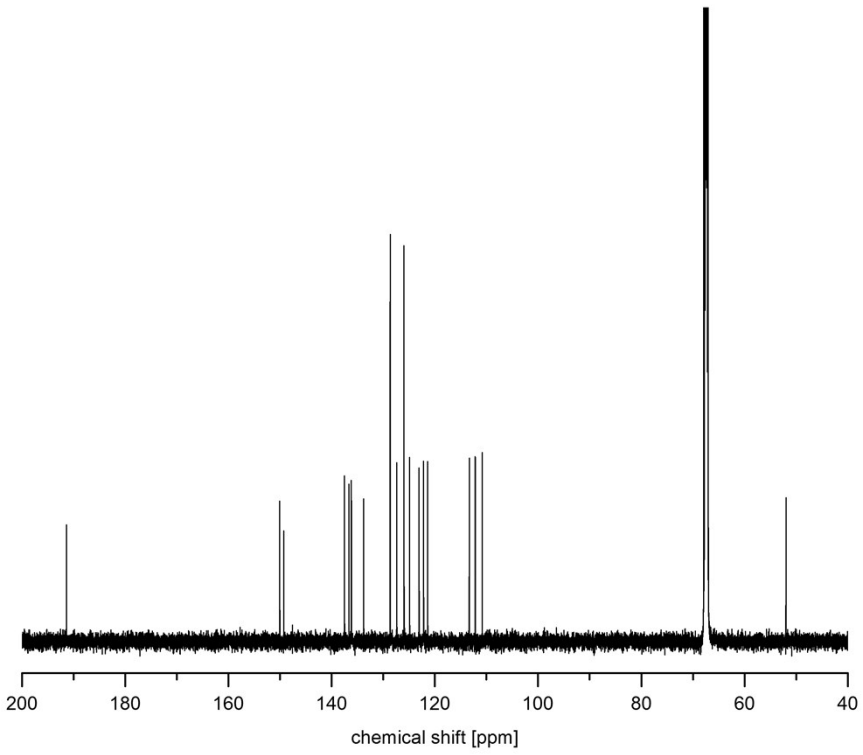

7.13. ^{1}H-NMR of *fac*-tris(*N*-phenyl,*N*-benzyl-benzimidazol-2-yl)iridium(III)

(2)

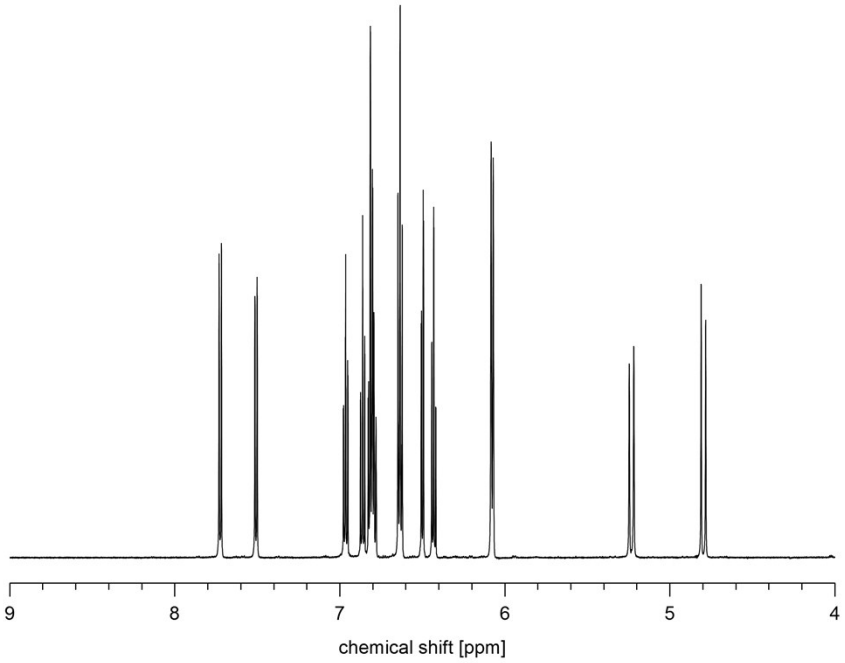

7.14. ^{13}C-NMR of *fac*-tris(*N*-phenyl,*N*-benzyl-benzimidazol-2-yl)iridium(III)

(2)

8. Optical properties of 1 and 2

8.1. Photoluminescence spectra of *mer*- and *fac*-1

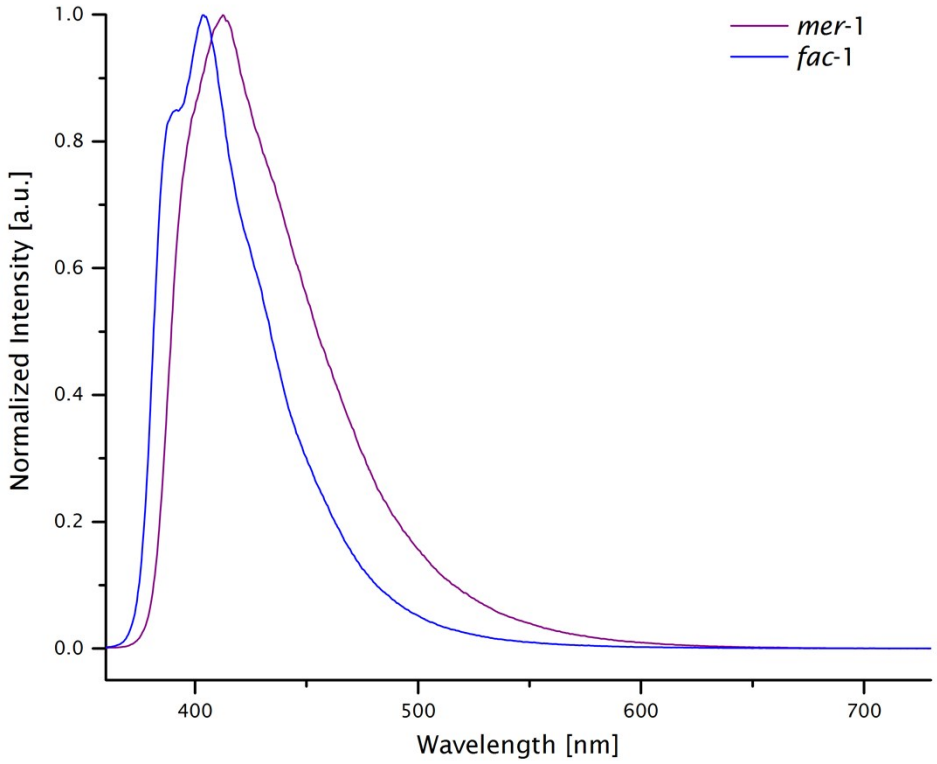

8.2. UV-Vis spectra of *mer*- and *fac*-1

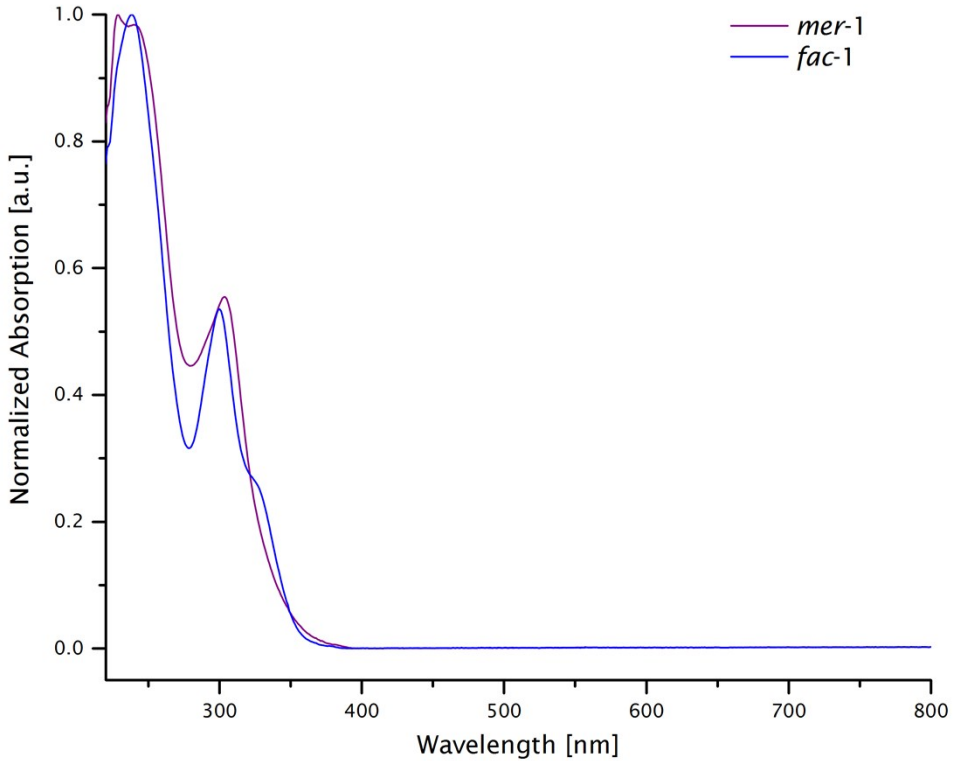

8.1. Photoluminescence spectra of *mer*- and *fac*-2

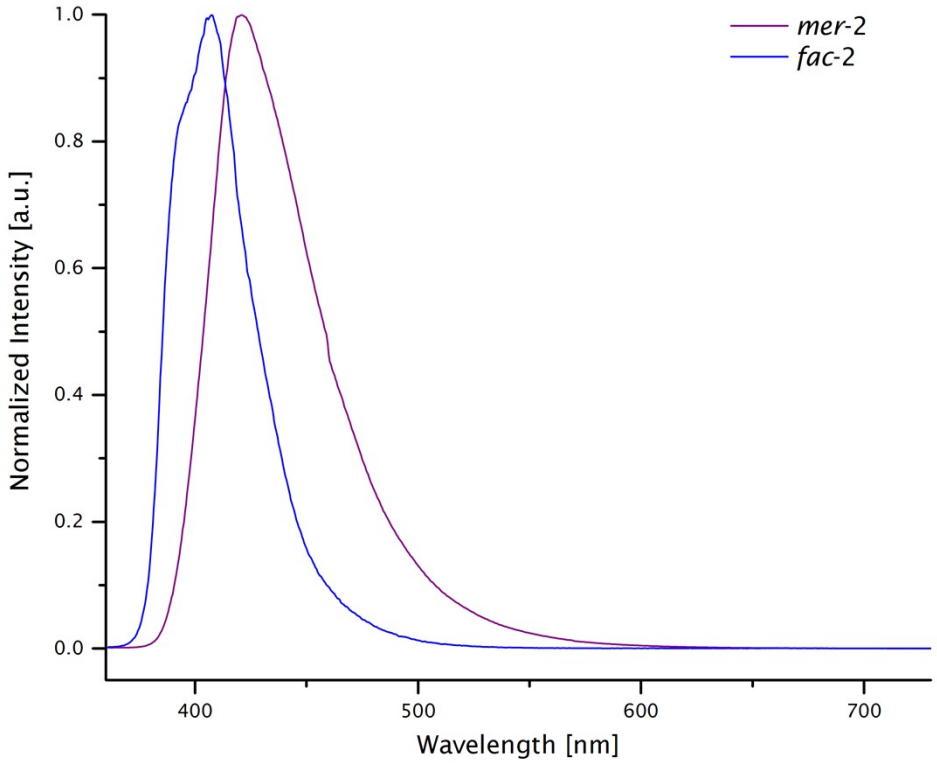

8.2. UV-Vis spectra of *mer*- and *fac*-2

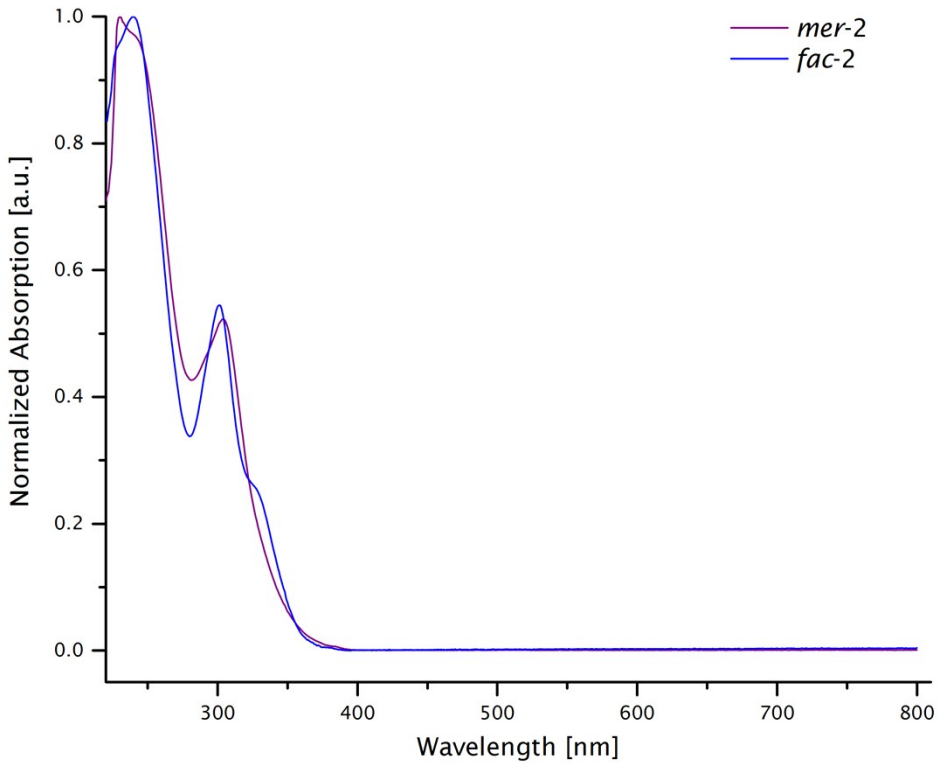

8.3. CIE-Diagram of *mer*-1/2 and *fac*-1/2

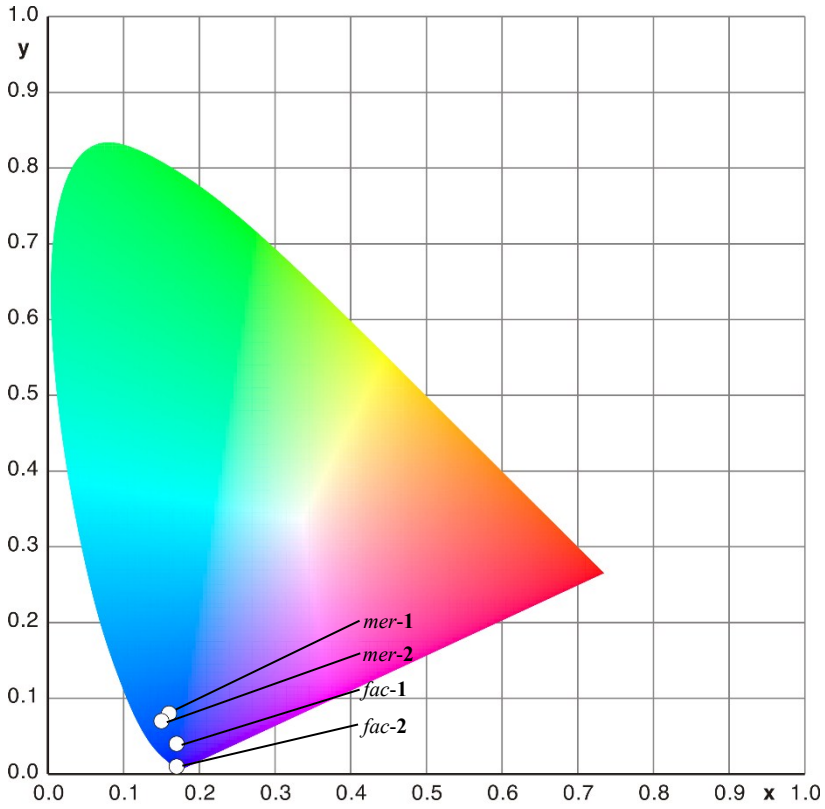

CIE 1931-coordinates
mer-**1**: x = 0.16 y = 0.08
fac-**1**: x = 0.17 y = 0.04
mer-**2**: x = 0.15 y = 0.07
fac-**2**: x = 0.17 y = 0.01

9. Literature

[1] T. Sajoto, P. I. Djurovich, A. Tamayo, M. Yousufuddin, R. Bau, M. E. Thompson, *Inorg. Chem*., **2005**, *44*, 7992–8003

[2] A. Tronnier, U. Heinemeyer, S. Metz, G. Wagenblast, I. Muenster, T. Strassner, *J. Mater. Chem. C*., **2015**, *3*, 1680–1693.

[3] J. G. Gordon, R. H. Holm, *J. Am. Chem. Soc.* **1970**, *92*, 5319–5332.

[4] S. Grimme, J. Antony, S. Ehrlich, H. Krieg, *J. Chem. Phys.* **2010**, *132*, 154104.

[5] a) F. Weigend, *Phys. Chem. Chem. Phys.* **2006**, *8*, 1057–1065; b) J. P. Perdew, *Phys. Rev. B* **1986**, *33*, 8822–8824.

[6] F. Weigend, R. Ahlrichs, *Phys. Chem. Chem. Phys.* **2005**, *7*, 3297–3305.

[7] A. D. Becke, *Phys. Rev. A* **1988**, *38*, 3098–3100.

[8] S. H. Vosko, L. Wilk, M. Nusair, *Can. J. Phys.* **1980**, *58*, 1200–1211.

[9] J. C. Slater, *Phys. Rev.* **1951**, *81*, 385–390.

[10] P. A. M. Dirac, *Proc. R. Soc. A* **1929**, *123*, 714–733.

[11] a) A. D. Becke, *J. Chem. Phys.* **1993**, *98*, 5648; b) C. Lee, W. Yang, R. G. Parr, *Phys. Rev. B* **1988**, *37*, 785–789.

[12] D. Andrae, U. Häußermann, M. Dolg, H. Stoll, H. Preuß, *Theoret. Chim. Acta* **1990**, *77*, 123–141.

[13] TURBOMOLE V7.0 2015, a development of University of Karlsruhe and Forschungszentrum Karlsruhe GmbH, 1989-2007, TURBOMOLE GmbH, since 2007; available from http://www.turbomole.com.

[14] a) F. Eckert, A. Klamt, *AIChE J.* **2002**, *48*, 369–385; b) A. Klamt, V. Jonas, T. Bürger, J. C. W. Lohrenz, *J. Phys. Chem. A* **1998**, *102*, 5074–5085; c) A. Klamt, *J. Phys. Chem.* **1995**, *99*, 2224–2235.

[15] COSMOtherm, C3.0, release 1501, COSMOlogic GmbH & Co KG, http://www.cosmologic.de.

[16] a) P. Deglmann, S. Schenk, *J. Comput. Chem.* **2012**, *33*, 1304–1320; b) P. N. Plessow, A. Schäfer, M. Limbach, P. Hofmann, *Organometallics* **2014**, *33*, 3657–3668.

[17] M. Amati, F. Lelj, *Chemical Physics Letters* **2002**, *363*, 451–457.

[18] E. M. S. Maçôas, R. Fausto, J. Lundell, M. Pettersson, L. Khriachtchev, M. Räsänen, *J. Phys. Chem. A* **2000**, *104*, 11725–11732.

[19] M. Merchán, F. Tomás, I. Nebot-Gil, *J. Mol. Struct.* **1984**, *109*, 51–60.

[20] S. Lünnemann, *Diploma Thesis*, Westfälische Wilhelms-Universität Münster, Münster, **2004**.

[21] A. D. Boese, M. Kirchner, G. A. Echeverria, R. Boese, *Chemphyschem* **2013**, *14*, 799–804.

[22] G. M. Sheldrick, *Acta Crystallogr., Sect. A: Found. Crystallogr.* **2008**, *64*, 112–122.